WIND- AND BUOYANCY-MODULATED ALONG-SHORE CIRCULATION OVER THE TEXAS-LOUISIANA SHELF

A Dissertation

by

ZHAORU ZHANG

Submitted to the Office of Graduate Studies of
Texas A&M University
in partial fulfillment of the requirements for the degree of

DOCTOR OF PHILOSOPHY

Chair of Committee,	Robert D. Hetland
Co-Chair of Committee,	Xiaopei Lin
Committee Members,	Ping Chang
	Achim Stössel
	Istvan Szunyogh
Head of Department,	Piers Chapman

August 2013

Major Subject: Oceanography

ABSTRACT

Numerical experiments are used to study the wind- and buoyancy-modulated along-shore circulation over the Texas-Louisiana continental shelf inshore of 50-m water depth. Most attention is given to circulation in the non-summer flow regime. A major focus of this study is on a unique along-shore flow phenomenon – convergent along-shore flows, which is controlled jointly by wind forcing and buoyancy fluxes from the Mississippi-Atchafalaya river plume. The second problem addresses the forcing effect of buoyancy on the general along-shore circulation pattern over the shelf in non-summer.

The convergent along-shore flows are characterized by down-coast flow from the northern shelf encountering up-coast flow from the southern shelf. This phenomenon is explored for both weather band and seasonal timescales. For the weather band, investigations are focused on non-summer convergent events. The formation of convergent flows is primarily caused by along-coast variation in the along-shore component of wind forcing, which in turn is due to the curvature of the Texas-Louisiana coastline. In general, along-shore currents are well correlated with along-shore winds. However, the points of convergence of currents and winds are not co-located, but rather, points of convergence of currents typically occur down-coast of points of convergence of wind. This offset is mainly caused by buoyancy forcing that forces down-coast currents and drives the point of convergence of currents further down-coast. No specific temporal shift pattern is found for the weather-band convergence, whereas monthly

mean convergence exhibits a prominent pattern of seasonal along-coast migration.

Buoyancy forcing in the non-summer along-shore flow is investigated in detail in the second part of this study. During non-summer, under down-coast wind forcing, the Mississippi-Atchafalaya river plume exhibits a bottom-advected pattern, for which isopycnals strongly interact with the sea floor. The density front is fairly wide and spans nearly across the entire shelf. Within the front, vertical shear of the alongshore flow is in thermal wind balance with the cross-shore density gradient, and the shear causes a slight reversal of alongshore flow near the bottom. An alongshore flow estimated by the thermal wind relation, along with an assumption of zero bottom reference velocity, agrees well with the actual alongshore flow.

ACKNOWLEDGEMENTS

I would like to express my deepest appreciation and gratitude to my committee chair, Dr. Robert Hetland, who provided me persistent guidance, support and help during my graduate study. Dr. Hetland is very rich intellectually and can always come up with brilliant ideas for conducting scientific research, expressing scientific thoughts and conveying scientific results. He also encouraged me to make independent thinking and gave me the freedom to explore on my own. He offered me several opportunities to participate in academic activities, which helped me to communicate with scientists in my research field and broaden my horizon. Without the mentorship of Dr. Hetland, this dissertation would not have been possible.

I would also like to thank my co-chair, Dr. Xiaopei Lin, and my committee members, Dr. Ping Chang, Dr. Achim Stössel and Dr. Istvan Szunyogh, for their patient instructions and thought-provoking suggestions on my research. I received the guidance from Dr. Lin from my undergraduate study, and I am very impressed by his wisdom in teaching, instructing and conducting scientific research. I have substantially benefitted from Dr. Chang's classes during my Ph.D. study. He is always nice to provide help, and I appreciate all the encouragements and insightful comments he offered for my study and research. I want to give my special thanks to Dr. Stössel, my former advisor, who taught me how to do research in the very beginning. I am grateful to him for his continuous guidance and detailed comments on my research work. I thank Dr. Szunyogh for the

long discussions that helped me sort out the technical details of data assimilation, which work is not included in this dissertation. I would like to thank Dr. Steve DiMarco for his kindness to substitute for Dr. Stössel in the dissertation defense and the useful comments he gave me on the Gulf of Mexico research.

I would like to thank my colleagues, Wenxia Zhang, Kelly Cole, Kristen Thyng, Xiaoqian Zhang, Zengrui Rong, Fei Chen and Martinho Marta-Almeida for their various forms of help during my graduate study. They provided a lot of useful advice for my research, and the discussions with them have dramatically improved my knowledge of coastal dynamics. I am also thankful to Steve Baum for maintaining the clusters so the modeling work can go smoothly.

I would like to thank my friends and the faculty in the Department of Oceanography for their encouragements and aids in my graduate study.

I would like to give my acknowledgement to all the agencies and people that provide datasets used in my dissertation, including the Geochemical and Environmental Research Group at Texas A&M University that provided the TABS buoy data, and Dr. Steve DiMarco who provided the Mechanisms Controlling Hypoxia data. All open access datasets are also appreciated.

I would like to thank the Texas General Land Office for funding my research project. I am grateful to Ocean University of China for providing me the opportunity to pursue my Ph.D. degree at Texas A&M University, and I want to thank the Chinese Scholarship Council for providing me financial support during the first four years of my Ph.D. study.

I would like to express my heart-felt gratitude to my family. My husband Yajie has provided me firm support during my graduate study and aided and encouraged me throughout this endeavor. I feel really sorry and grateful for my daughter Grace, who has to stay in China with her grandparents in this semester so I can concentrate on my dissertation writing and get all the work done. I am also very thankful to my parents and parents-in-law for helping me take care of Grace.

TABLE OF CONTENTS

Page

LIST OF FIGURES

Page

LIST OF TABLES

Page

CHAPTER I

INTRODUCTION

The Texas-Louisiana shelf (Figure 1) is located in the northwestern Gulf of Mexico, and is an economically important coastal region due to extensive offshore oil and gas activities, dense ship traffic serving major ports, commercial and sport fishing, and coastal tourism. The shelf circulation influences industry activities and biogeochemical processes in this region, such as oil spill trajectories, the initiation and movement of harmful algal blooms [*Hetland and Campbell*, 2007] and the occurrence of seasonal hypoxia [*Bianchi et al.*, 2010; *DiMarco et al.*, 2010]. Therefore, extensive studies have been conducted to explore the mechanisms controlling the flow dynamics on the shelf.

It has been demonstrated in previous studies that the major forcing mechanisms for the Texas-Louisiana shelf circulation are wind, buoyancy fluxes from the Mississippi-Atchafalaya fresh water discharge and offshore eddies from the Loop Current [*Cho et al.*, 1998; *Cochrane and Kelly*, 1986; *Li et al.*, 1996; *Nowlin et al.*, 2005; *Oey*, 1995]. *Nowlin et al.* [2005] divided the shelf into an inner shelf region, inshore of the 50-m isobath, and an outer shelf region, offshore of the 50-m isobath to the shelf break. Currents over the inner shelf are primarily modulated by wind and buoyancy fluxes, while flows over the outer shelf are also frequently influenced by the offshore Loop Current eddies. This study focuses on the along-shore circulation over the Texas-Louisiana shelf inshore of 50-m water depth, and most attention will be given to the non-

summer flow regime, when ocean currents are more energetic, and some flow features, as will be discussed below, are more prominent. The overall objective is to identify the role of wind forcing and buoyancy fluxes in the along-shore flow dynamics.

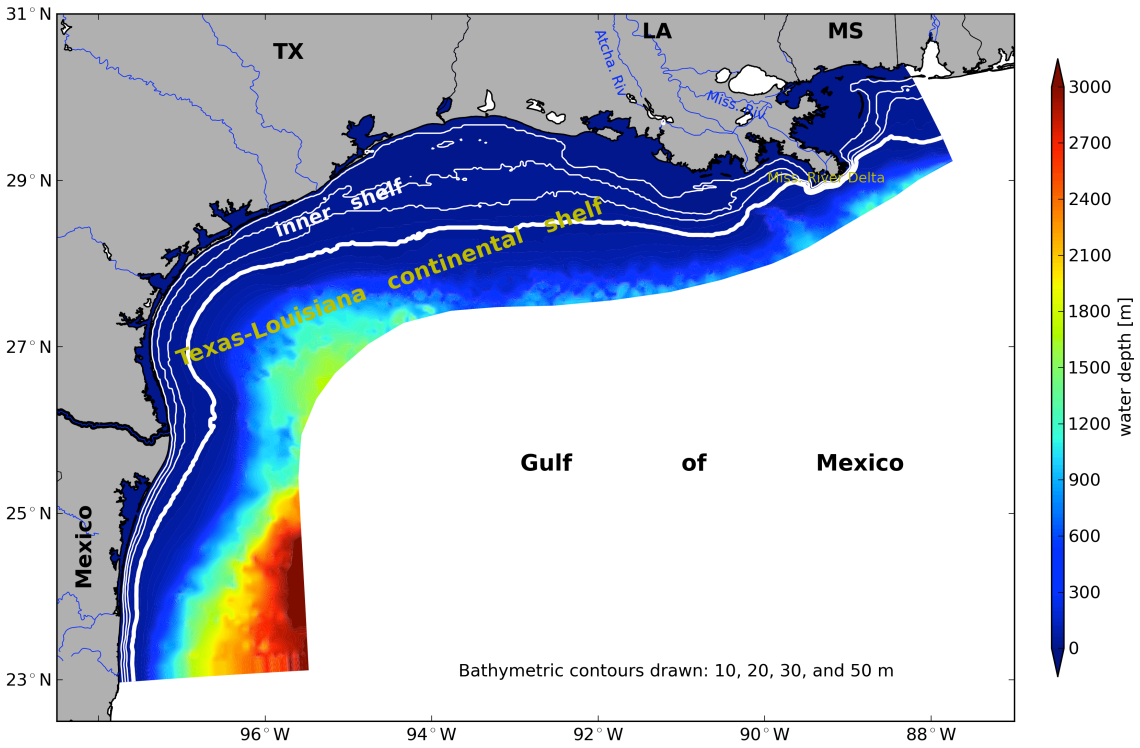

Figure 1. Map of the northwestern Gulf of Mexico. The colors show the bathymetry of the Texas-Louisiana continental shelf up to 3000 m. The bathymetric contours of 10, 20, and 30 m are drawn with thin, white lines. The thick, white line marks the 50-m isobath, which partitions the shelf into an inner-shelf region and an outer-shelf region. The blue lines indicate the major rivers flowing into the Texas-Louisiana shelf, including the Mississippi River and the Atchafalaya River.

1.1 Background

1.1.1 Forcing mechanisms of wind and buoyancy of the along-shore flow on a continental shelf

1.1.1.1 Wind

Wind, particularly the along-shore wind, has been demonstrated to be the most important forcing mechanism of currents on an un-stratified continental shelf. The effect of along-shore wind on shelf flows has been extensively studied, and it is widely accepted that the along-shore wind drives along-shore currents via a coastal set-up or set-down of the sea level. The mechanism is schematized in Figure 2. Downwelling-favorable (or down-coast, and for the Texas-Louisiana shelf, this direction is from Louisiana to Texas) wind drives onshore Ekman flows, which are blocked by the coast and results in a coastal set-up of the sea level. The cross-shore pressure gradient generates a geostrophic flow that follows the same direction as the wind [*Lentz and Fewings*, 2012]. Similarly, an upwelling-favorable (or up-coast, and for the Texas-Louisiana shelf, this direction is from Texas to Louisiana) wind drives an up-coast geostrophic flow via offshore Ekman transport and a coastal set-down of the sea level. The above processes occur in water deep enough to allow a separation of the surface and bottom boundary layers and a significant role of rotation in the flow dynamics. In very shallow water where the surface and bottom boundary layers overlap and the rotational effect is small, the along-shore

wind directly drives an along-shore flow through a frictional balance between the wind stress and the bottom stress [*Csanady*, 1978; *Lentz and Fewings*, 2012; *Whitney and Garvine*, 2005].

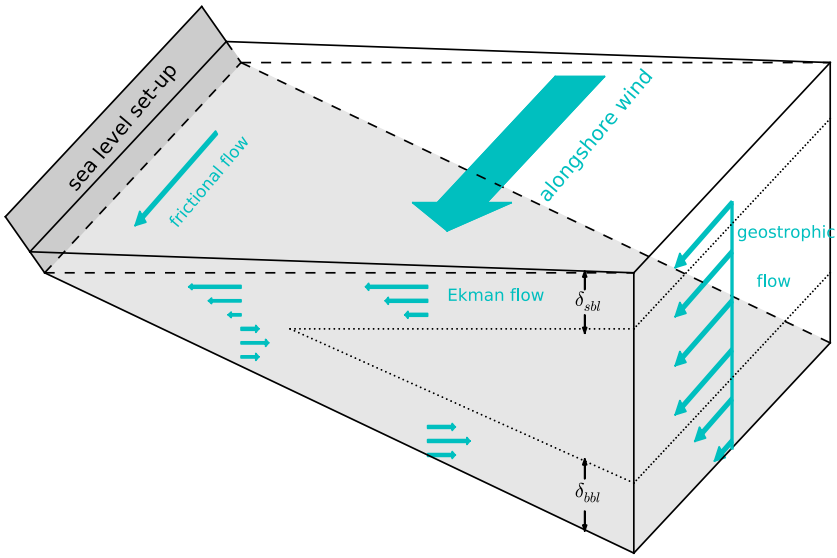

Figure 2. Schematic of a down-coast wind driving along-shore currents on an un-stratified continental shelf (adapted from *Chapman and Lentz* [1994]). The down-coast wind generates an onshore Ekman transport, which is blocked by the coast and results in a coastal set-up of the sea level. The corresponding cross-shore pressure gradient drives a geostrophic flow that is in the same direction as the along-shore wind. In very shallow water where the surface boundary layer (sbl) overlaps the bottom boundary layer (bbl), the along-shore wind drives a frictional along-shore flow.

1.1.1.2 Buoyancy fluxes

Buoyant inflow from river discharge is another important forcing mechanism for shelf currents. Fresh water inflow encounters ambient shelf water and forms a low-salinity plume that separates the buoyant brackish river water from shelf water with a sharp

density gradient. The density gradient, which is positive offshore, tends to drive a down-coast current through the thermal wind relation. The buoyancy forcing mechanism is schematized in Figure 3.

Yankovsky and Chapman [1997] classified river plumes into three types - surface-advected plume, bottom-advected plume and intermediate plume, based on the interaction of the plume with the sea floor. For the surface-advected plume, the buoyant water stays in the surface ocean with ambient denser shelf water beneath it, and the plume spreads offshore with little contact with the bottom unless near the coast. For the bottom-advected plume, the buoyant water can occupy the entire water column, and the plume has strong interaction with the sea floor. An intermediate plume falls between the surface- and bottom-advected plumes.

The cross-shore structure of the plume, and thus the buoyancy-driven currents, can be substantially modulated by winds [*Whitney and Garvine*, 2005]. Downwelling favorable winds compress the plume against the coast through onshore surface Ekman transport; this steepens the isopycnals and can create a bottom-advected plume pattern (Figure 3). On the contrary, upwelling favorable winds stretch the plume off the coast through offshore surface Ekman transport; this decreases the isopycnal slope [*Fong et al.*, 1997; *Sanders and Garvine*, 2001; *Whitney and Garvine*, 2005] and creates a surface-advected plume pattern. It is expected that under different plume patterns, the role of buoyancy forcing in the along-shore flow dynamics will change due to changing density field. One

target scientific problem of this study is the buoyancy forcing effect on along-shore flows in non-summer, when the Mississippi-Atchafalaya river plume is strained by down-coast wind and has a bottom-advected pattern, as will be shown below.

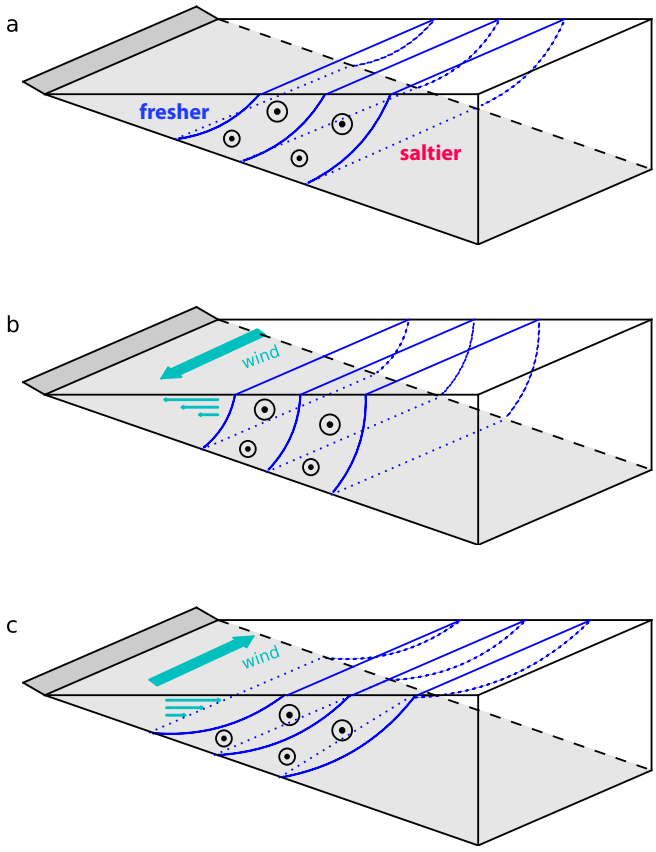

Figure 3. Schematic of (a) the forcing mechanism of a buoyant plume for along-shore currents and (b-c) the along-shore wind straining on the plume pattern and the related density field. The buoyant plume sets up a horizontal density gradient that is positive offshore, which tends to drive a down-coast flow through a thermal wind relation (a). Under (b) down-coast wind forcing, the onshore Ekman transport steepens the isopynals and creates a bottom-advected plume. Under (c) up-coast wind forcing, the offshore Ekman transport tilts the isopycnals and creates a surface-advected plume.

1.1.2 General patterns of wind and buoyant plume on the Texas-Louisiana shelf

1.1.2.1 Wind pattern

Wind over the Texas-Louisiana shelf has widely varying temporal scales. The seasonal wind is characterized by an annual cycle: in non-summer months (typically from September to May) northerly or northeasterly winds prevail over the shelf, while in summer months (June through August) southerly or southeasterly winds become dominant (Figure 4) [*Wang et al.*, 1998]. Therefore the along-shore component of wind experiences a reversal from down-coast during non-summer to up-coast during summer. The shift of wind from the non-summer to summer pattern occurs first at the Mexican border in early spring and migrates north- and eastward along the coast in spring and summer. Beginning in late August or early September, the wind shifts back to the non-summer pattern first over the eastern shelf, and this shift migrates south- and westward along the coast during fall and winter. Such wind shift pattern creates a line where the along-shore winds converge. This convergence feature will be discussed in Chapter II. The seasonal wind has interannual variability in terms of dominance time and strength of the non-summer and summer wind patterns; for example, the winds in year 2009 are reported to have a much stronger up-coast component during summer months than average [*Feng et al.*, 2012].

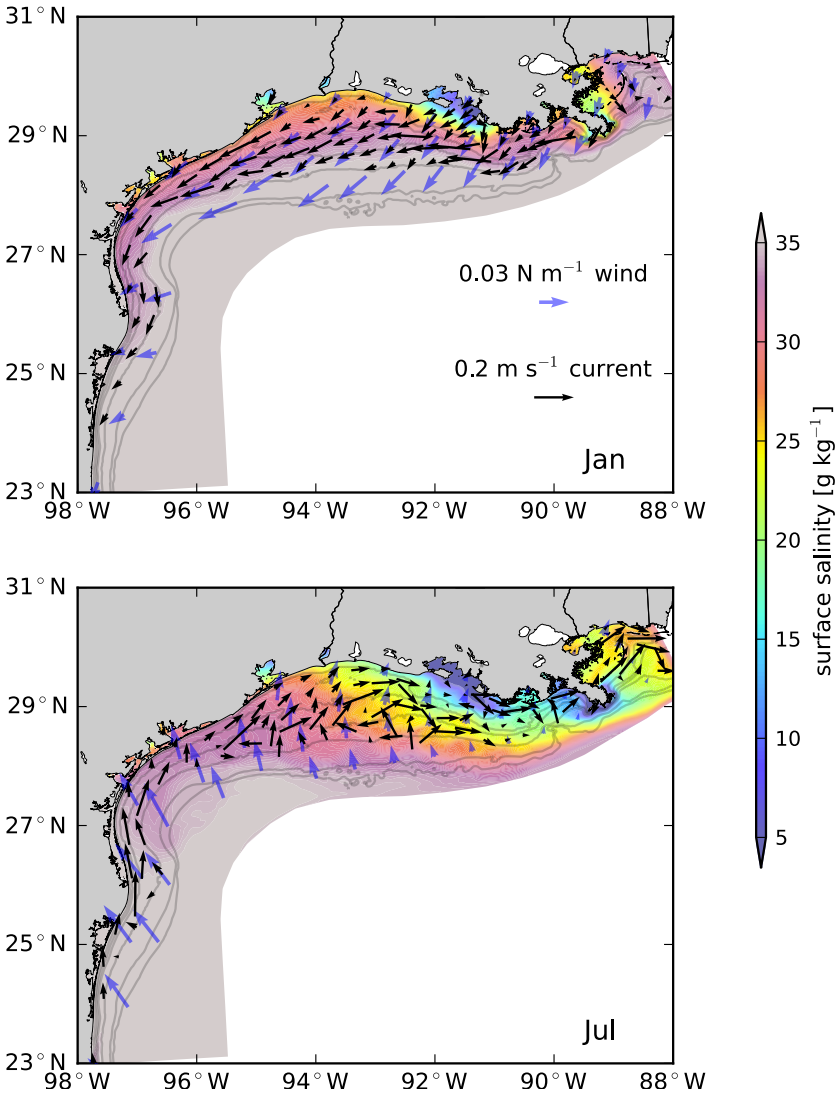

Figure 4. Monthly mean surface wind stress (blue arrows), currents (black arrows) and salinity (color) fields over the Texas-Louisiana shelf for (upper) January and (lower) July of 2011 based on simulation of a high-resolution model covering the Texas-Louisiana shelf and slope region (The model is described in 3.2).

Wind in the weather band is characterized by extreme events, such as cold fronts, cyclogenesis and hurricanes [*Nowlin*, 1998; *Wang et al.*, 1998]. Passage of cold fronts occurs frequently over the Texas-Louisiana shelf during fall and winter months, with a

frequency of 4-7 per month; in summer, their occurrence is much less. Under a cold front, the wind speed can increase from ~ 5 m s^{-1} to ~ 15 m s^{-1} [*Nowlin et al.*, 2005; *Wang et al.*, 1998]. The influence of frontal passages on the weather band convergence phenomenon in winter will be discussed in Chapter II. In the weather band, winds in nonsummer are typically more variable in direction than in summer, and thus seasonal mean winds in non-summer can be weaker than in summer [*Wang et al.*, 1998]. The most important high-frequency feature of wind over the Texas-Louisiana continental shelf is the land-sea breeze, which is caused by diurnal heating of the land surface in summer and the corresponding cyclic onshore-offshore wind flows generated by thermal gradient [*Zhang et al.*, 2009].

1.1.2.2 Pattern of the Mississippi-Atchafalaya River plume

The Mississippi River (Figure 1) is the major source of fresh water input into the Texas-Louisiana shelf. The annual average discharge of the Mississippi River is ~ 19,000 m^3/s [*Wiseman et al.*, 1997], and nearly thirty percent of the total discharge is delivered to the Texas-Louisiana shelf by the Atchafalaya River (Figure 1), a distributary of the Mississippi River in Louisiana. The other seventy percent of discharge enters the Gulf of Mexico through the Mississippi River Delta [*Jarosz and Murray*, 2005]. With earth's rotation, fresh water coming from the Mississippi-Atchafalaya river mouths turns right and forms a low-salinity plume on the Texas-Louisiana shelf (Figure 4). During non-summer seasons, the plume is confined to the coast by down-coast wind and is carried

down the shelf (downcoast) by buoyancy- and wind-driven down-coast currents; it can reach as far southwest as the east Mexico shelf. During summer seasons, the up-coast component of wind pools the fresh water towards the Louisiana shelf and increases the plume width in this region [*Cochrane and Kelly*, 1986; *Morey et al.*, 2005; *Zhang et al.*, 2012a]. Such change in the plume pattern would cause a change in the cross-shore density structure. Therefore, the forcing effect of buoyancy on the along-shore flow will be different in non-summer and summer.

1.1.3 General patterns of circulation over the inner Texas-Louisiana shelf

Similar to the wind forcing, circulation over the Texas-Louisiana shelf occurs on a wide range of temporal scales. Corresponding to the annual cycle of wind, the seasonal circulation over the Texas-Louisiana shelf undergoes an annual reversal as well. Currents over the inner shelf flow down-coast in non-summer months and up-coast in summer months (Figure 4) [*Cho et al.*, 1998; *Cochrane and Kelly*, 1986; *Jarosz and Murray*, 2005; *Li et al.*, 1996; *Nowlin et al.*, 2005]. The shift of currents between the non-summer and summer patterns follows closely that of wind: the up-coast component of current first appears in late winter over the southwestern shelf and develops toward the northern and eastern shelf with time until dominating most of the shelf in mid-summer; the down-coast component of current first appears over the northeastern shelf in early fall and develops toward the southern and western shelf with time until dominating most of the shelf in mid-winter. Similar to the wind pattern, a convergence

region exists in the flow field where up-coast flows encounter down-coast flows. Convergence in the seasonal along-shore circulation over the Texas-Louisiana shelf will be discussed in Chapter II.

Circulation in the weather band is mainly influenced by atmospheric events, particularly frontal passages. Currents over the inner shelf have a fast response to the passage of cold fronts, and are typically intensified in the down-coast direction under the forcing of strong down-coast wind component [*Nowlin et al.*, 2005]. The cold-front-induced currents contribute to the down-coast component of the seasonal mean flow in wintertime. In the near-inertial band, a coincidence of the frequency of land-sea breeze and the local inertial frequency on the Texas-Louisiana shelf generates an energetic near-inertial oscillation in the flow field. The near-inertial motions are characterized by clockwise rotating horizontal flows with a cycle of ~24 hours [*Zhang et al.*, 2009; *Zhang et al.*, 2010]. The major interest of this study is in the subinertial currents, and thus in most analyses the near-inertial motions will be removed by a 33-hr low-pass filter.

1.2 Scientific problems and objectives

This dissertation targets two scientific problems associated with the wind- and buoyancy-modulated along-shore circulation over the Texas-Louisiana shelf inshore of the 50-m isobath. First: convergent along-shore currents, a unique flow phenomenon on the Texas-Louisiana shelf that occurs frequently in non-summer seasons. It will be

shown in Chapter II that the character of this phenomenon is controlled jointly by along-shore wind and buoyancy forcing. Second: a more detailed investigation of the buoyancy forcing effect on the general along-shore circulation in non-summer. This will be dealt with in Chapter III. Both phenomena are briefly described below.

1.2.1 Convergent along-shore flows

Concerning the Texas-Louisiana shelf circulation, an interesting feature that has been noted in previous studies is convergence (or called 'confluence' in some studies) in the along-shore coastal flows. This phenomenon is characterized by down-coast flows along the northern section of the shelf encountering up-coast flows along the southern section of the shelf. The convergent along-shore flows were first noted in the 1950s through ship's drift information [*Leipper*, 1954]. Its existence was further supported in the 1970s by drift bottle studies [*Hunter et al.*, 1974; *Watson and Behrens*, 1970]. *Cochrane and Kelly* [1986] found a line of convergence in the monthly mean field of along-shore wind stress, and they inferred that a convergence should exist in the along-shore currents as well. Such inference was then confirmed in numerical studies of seasonal circulation in the western Gulf of Mexico by *Morey et al.* [2005] and *Zavala-Hidalgo et al.* [2003], but they did not really focus on this feature and the corresponding controlling mechanisms.

Convergence phenomena have also been noted on other continental shelves. For example, *Yuan et al.* [2005] suggested that cross-shelf penetrating fronts observed off

the southeast coast of China might be associated with the convergence of two current systems flowing in opposing directions. The reason for this study to focus on the convergent flows is that such flows can concentrate floating material near the coast, and are thus important for understanding and predicting shoreline impacts of oil spills, as well as harmful algae bloom initiation and subsequent transport [*Hetland and Campbell*, 2007]. Compared to previous research, this study aims to provide a deeper insight into the convergent flow phenomenon. The objectives include (1) identifying the primary mechanism for the formation of convergent flows, (2) identifying the factors that control the location of convergent flows and (3) characterizing the temporal shifts in the convergence location.

1.2.2 Buoyancy-driven seasonal along-shore circulation in the non-summer flow regime

In the first part of this study, i.e. the convergent along-shore flows, the along-shore circulation is considered as wind-driven flow modified by buoyancy, as will be shown in Chapter II. In the second part of this work, the along-shore flow will be considered as buoyancy-driven flow influenced by wind. The along-shore circulation on seasonal timescales has been the objective of many studies on the Texas-Louisiana shelf flow dynamics since the 1980s, but most of them emphasized the direct forcing effects of along-shore wind, and none has considered the currents as buoyancy-driven flows, where wind plays a role in modulating the buoyancy structure. In the context of a coastal

plume, several studies take the buoyancy-driven flow as a background along-shore flow [*Whitney and Garvine*, 2005], which can be modified by along-shore wind. It is natural for us to consider the circulation on the Texas-Louisiana shelf inshore of 50-m water depth in the same way, given that it is within the reach of the Mississippi-Atchafalaya river plume, the largest fresh water plume in the U.S. coastal areas. Therefore, this study will emphasize the forcing effect of buoyancy on along-shore flow over the shelf, and the buoyancy forcing is explored in the context of realistic wind.

Buoyancy forcing drives along-shore flow through a thermal wind relation, that is, a vertical shear exists in the along-shore flow field due to the large cross-shore density gradient set up by the river plume. The thermal-wind-balance-derived flow should therefore be an important component of the actual along-shore flow. As described in section 1.1.1.2, the plume structure and related density field are influenced by along-shore wind forcing. The non-summer flow regime of the Texas-Louisiana shelf is dominated by down-coast wind, which tends to create a bottom-advected pattern of the Mississippi-Atchafalaya river plume. The primary objective of this study is to investigate in the bottom-advected river plume, how much of the seasonal along-shore flow on the Texas-Louisiana shelf can be explained by the thermal-wind-balance-derived flow.

CHAPTER II

CONVERGENT ALONG-SHORE FLOWS OVER THE TEXAS-LOUISIANA SHELF[*]

2.1 Background

The possible mechanism for the formation of convergent flows in seasonal circulation has been briefly discussed in previous studies. *Cochrane and Kelly* [1986] proposed a conceptual model to explain the formation of convergence: with uniform wind stress blowing toward the coast of the northwestern Gulf, the curvature of the coastline creates a change in direction of the along-shore wind stress. Since on seasonal timescale, along-shore currents typically flow in the direction of the along-shore wind stress, the convergence in along-shore wind creates a convergence in along-shore current. *Morey et al.* [2005] and *Zavala-Hidalgo et al.* [2003] also suggested that convergent flows occur as a result of change in the sign of along-shore wind caused by the bending of the coastline.

All of the previous studies on the Texas-Louisiana shelf convergent flows focused on seasonal timescales. However, there is a substantial need to understand these flows at much shorter timescales. Oil spill and harmful algal bloom trajectory prediction requires

---

[*] Reprinted with permission from "A numerical study on convergence of alongshore flows over the Texas-Louisiana shelf" by Zhaoru Zhang and Robert Hetland, 2012. Journal of Geophysical Research, 117, C11010, Copyright [2012] by John Wiley and Sons.

predicting flow on timescales of days. Therefore, this study will focus more on the weather-band convergence that has not been discussed before, while seasonal convergence is also included as an extension of previous work. Also, previous studies only analyzed the relationship between convergent flows and local wind forcing; other factors affecting the shelf currents, such as buoyancy forcing, were not considered. Buoyancy effects are shown below to influence the convergence location.

2.2 Numerical model

It is difficult to study the convergence phenomenon using existing observations on the Texas-Louisiana shelf, due to the fact that these observations do not have either sufficient spatial or temporal resolution to resolve the locations of convergence. Therefore, a numerical simulation is the most appropriate tool for this investigation.

2.2.1 Model setup

The model employed to study the convergent flows is based on the Regional Ocean Modeling System (ROMS). ROMS is a free-surface, terrain-following hydrodynamic and primitive equations ocean model widely used in regional oceanic studies [*Shchepetkin and McWilliams*, 2005]. The model grid covers the entire Gulf of Mexico with uneven horizontal grid spacing (Figure 5, upper). The highest resolution is in the northwestern section of the Gulf with grid spacing of 4 km; in the southeastern Gulf the

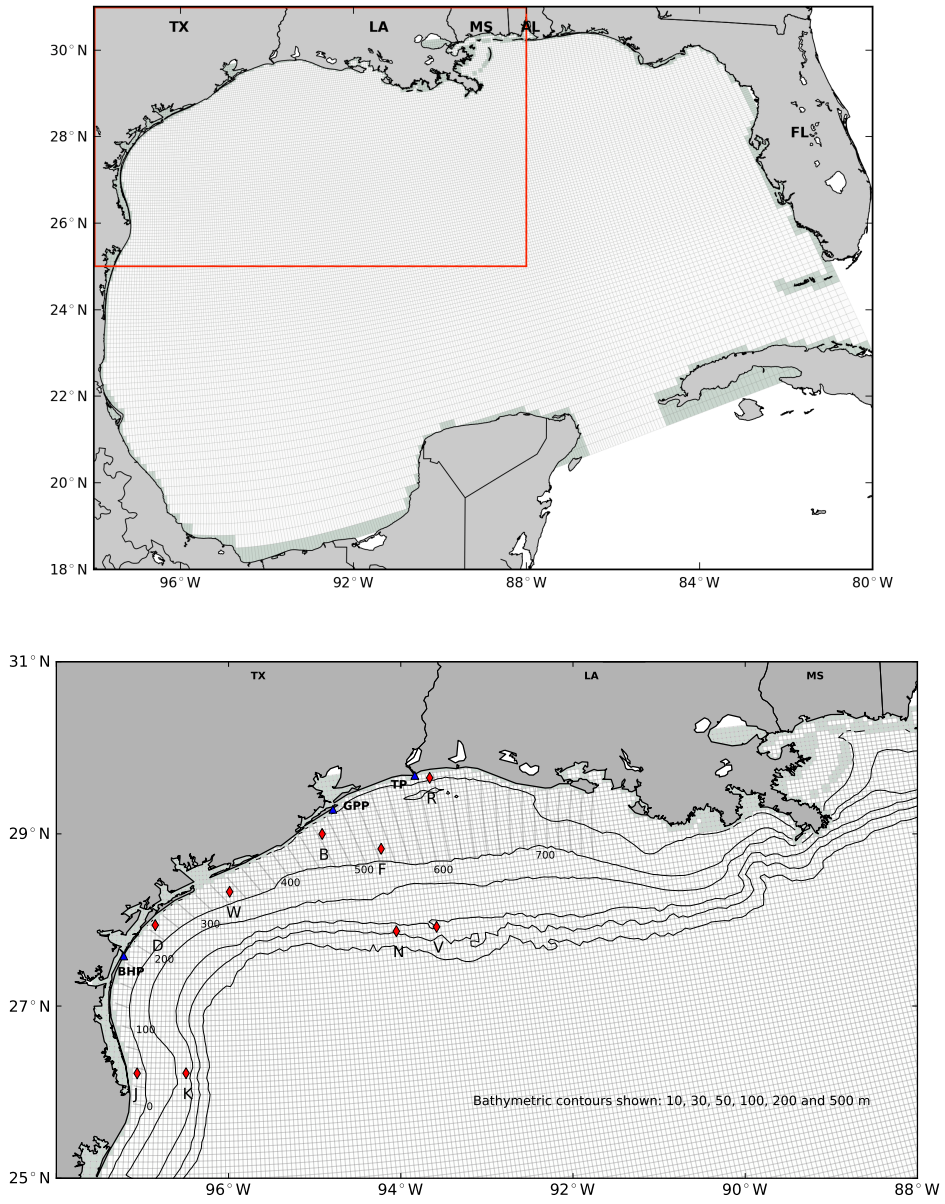

Figure 5. Geographic map showing the grid of the numerical model described in section 2.2. The model grid covers the entire Gulf of Mexico (upper panel); the red box marks the region of northwestern Gulf, which is enlarged in the lower panel. The bathymetric contours are shown for the 10, 30, 50, 100, 200 and 500 m isobaths. The light green squares indicate the land grids of the model. The TABS buoy sites are marked with red diamonds and the TCOON stations (Bob Hall Pier (BHP), Galveston Pleasure Pier (GPP) and Texas Point (TP)) are marked with blue triangles. Also plotted are the cross-shore transects from the south Texas coast to the central Louisiana coast that will be used in the analysis in Chapter II. The along-coast distance (in kilometers) of these transects to the origin (the southernmost transect) is labeled at 100-km intervals. Here, a transect is noted by its location, e.g., the 100-km transect refers to the transect at a distance of 100 km from the origin.

resolution is relatively coarse and approximately 15 km. The model has 10 vertical layers irregularly spaced between the surface and bottom (with a surface stretch parameter (θ_s) of 5.0, bottom stretch parameter (θ_b) of 0.8 and critical depth of 5.0 m; the terminologies are referred to *Haidvogel et al.* [2000]). The northern and western model boundaries are closed with no-slip boundary conditions, while the southern and eastern boundaries are open at the Yucatan Channel and Florida Straits, respectively. At the open boundaries, a Chapman condition [*Chapman*, 1985] is used for surface elevation and a Flather condition [*Flather*, 1976] is used for 2-D momentum equations. Radiation conditions are used for 3-D momentum equations and tracers. The model does not attempt to reproduce the Loop Current system by inducing a western boundary current flow through the Yucatan Channel and Florida Straits. As shown below in the model-data comparison, the wind and river forcing are the dominant forcing mechanisms driving currents inshore of 30-m water depth, the primary focus region of this study. Near the open boundaries, climatological nudging is applied to tracers and 3-D velocities. Temperature and salinity are nudged to horizontally uniform monthly climatological values and 3-D velocities are nudged to zero values to suppress the development of instability eddies. The nudging timescale for both tracers and velocities is 1 day at the outermost layer and increases toward the inner layers. The baroclinic time step is set to be 200 s, and the barotropic time step is 25 times shorter. The model is configured with a third-order upstream advection scheme for horizontal discretization and a conservative parabolic spline reconstruction for computing vertical gradient. A recursive multidimensional positive definite advection transport algorithm is used for

horizontal advection of tracers. Horizontal mixing of both momentum and tracers takes the Laplacian scheme, and turbulence closure is given by the Mellor-Yamada 2.5 scheme [*Mellor and Yamada*, 1982]. Bottom stress is parameterized with a quadratic drag law with a drag coefficient of 3×10^{-3}.

The model is initialized on January 1, 2000 with zero velocity and horizontally uniform climatological profiles for temperature and salinity based on historical hydrographic surveys. The total model integration time is 11 years. Atmospheric forcing includes 3-hourly u- and v- components of wind speed at 10-m height, shortwave radiation, air temperature, air pressure, relative humidity, cloud and precipitation from the North American Regional Reanalysis (NARR) dataset. The spatial resolution of this dataset is 32 km. Longwave radiation, sensible and latent heat fluxes are computed internally within ROMS using bulk formulations. The model is forced by fresh water discharge from the Mississippi and Atchafalaya rivers based on daily measurements of Mississippi River transport at Tarbert Landing conducted by the U.S. Army Corps of Engineers. This model does not contain tides, since previous studies have shown that tides are generally weak on the Texas-Louisiana shelf and only make a small contribution to the sea surface elevation and coastal currents [DiMarco and Reid, 1998]. In this research, the simulation with the model configuration described above is referred to as the reference run, and most of the subsequent analysis is based on the reference run. To investigate the effect of buoyancy forcing on the location of convergent flows, a

sensitivity run that has the river forcing taken out is also performed. The other aspects of the configuration for the sensitivity run are exactly the same as in the reference run.

2.2.2 Model assessment

2.2.2.1 Surface current simulations

The performance of the model in reproducing observed currents, salinity and surface elevation fields is evaluated against observational data. The simulated surface currents are compared with buoy measurements provided by the Texas Automated Buoy System (TABS, http://tabs.gerg.tamu.edu/). TABS is a coastal network of moored buoys that report near real-time observations of surface currents and winds along the Texas coast. Its primary mission is to provide ocean observations for oil spill response. Currents and temperature are measured 2-m below the surface every 30 minutes. Currently TABS consists of nine active sites, seven along the Texas coast and two offshore (Figure 5, bottom). Figure 6 shows the comparison between the modeled and observed surface along-shore velocities at the TABS buoy sites for year 2006. Model skill and the correlation coefficient between modeled and observed values are provided for each buoy. The model skill is defined as:

$$skill = 1 - \frac{\sum_{i=1}^{i=N} (d_i - \Im(m)_i)^2}{\sum_{i=1}^{i=N} (d_i - c_i)^2}, \qquad (1)$$

where d_i is the i th element of observations, m are model results that are converted to observational space by a linear operator $\Im$ (typically $\Im$ is taken as a linear interpolator in space and time), c are climatological values, and N is the number of total observations [*Bogden et al.*, 1996; *Hetland*, 2006]. In this study, the climatological values are computed from the buoy data and defined as monthly mean values averaged over year 2000 through 2009. From equation 1, if the model error (the numerator in the summation) is smaller than the variance of observations (the denominator) at a buoy location, then the model skill is positive.

Figure 6 shows that for most buoys, the model is able to capture the variability of the observed surface along-shore currents on seasonal timescales as well as on the weather band. Positive model skill indicates that the model is a more accurate representation of observations than climatology. The near-shore buoys, such as buoys B, D, J, R and W, all have relatively higher model skills because the along-shore flows near the coast are primarily driven by winds. On the other hand, the offshore buoys, such as buoy K, N and V, have negative or very low model skills as a result of the influence of offshore eddies, which are not represented in the current model setup; this model does not contain a Loop Current or Loop Current Eddies. For the near-shore buoys, coherence between the modeled and observed along-shore currents is generally high (between 0.7 and 0.8) for the seasonal scale, while for the weather band there is more variability in the coherence. However, power spectra (not shown) for modeled and observed currents are similar for the weather-band and lower-frequency variability, with discrepancies well within the

error of the spectra. This indicates that the model is able to capture the magnitude of the variability of currents on the weather band.

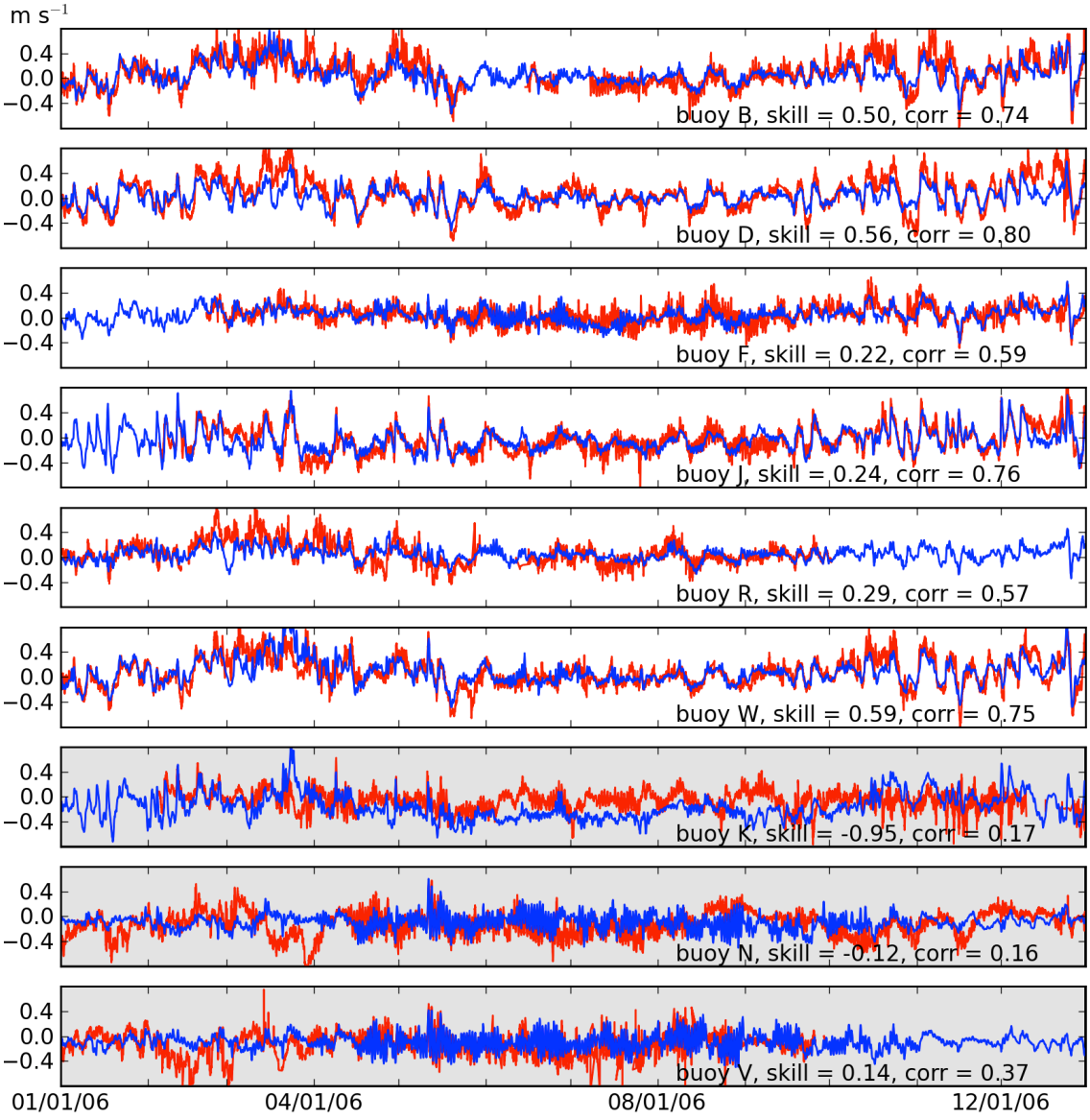

Figure 6. Comparison of surface along-shore currents between the model simulations (blue lines) and TABS buoy measurements (red lines) for the year 2006. The values of model skill and correlation are provided. Panels for the offshore buoys are shaded.

2.2.2.2 Salinity field assessment

Two independent datasets are used for evaluating the model salinity field. The first one is from the Southeast Area Monitoring and Assessment Program (SEAMAP). SEAMAP is a program administered by the Gulf States Marine Fisheries Commission for collection, management and dissemination of fisheries related scientific data. One of the operational components of the program is dedicated to the Gulf of Mexico and started back in 1981. It regularly collects fishery and environmental data, including temperature and salinity vertical profiles along the Texas-Louisiana continental shelf [*Marta‐Almeida et al.*, 2013]. In this study, the SEAMAP data used are salinity measurements collected during May, June and July of 2005 through 2008. This includes 1003 measurement profiles. For the model skill assessment (Figure 7), only data in the upper 50 m of water column are used, and the error presented for each profile is the vertically averaged value normalized by the standard deviation of data on this profile. The climatological data used here and for the second dataset are defined by the average of all historical hydrographic data available at the National Ocean Data Center, the same as those used in *Hetland and DiMarco* [2011]. Profiles of salinity are spatially and temporally averaged to provide a horizontally uniform monthly climatology over one year. Figure 7 shows that at the majority portion of observational sites the model error is smaller than the data variability; the model skill is positive for all the separate SEAMAP data collection periods, and on the whole the model skill exceeds 0.5 (Figure 7, bottom right).

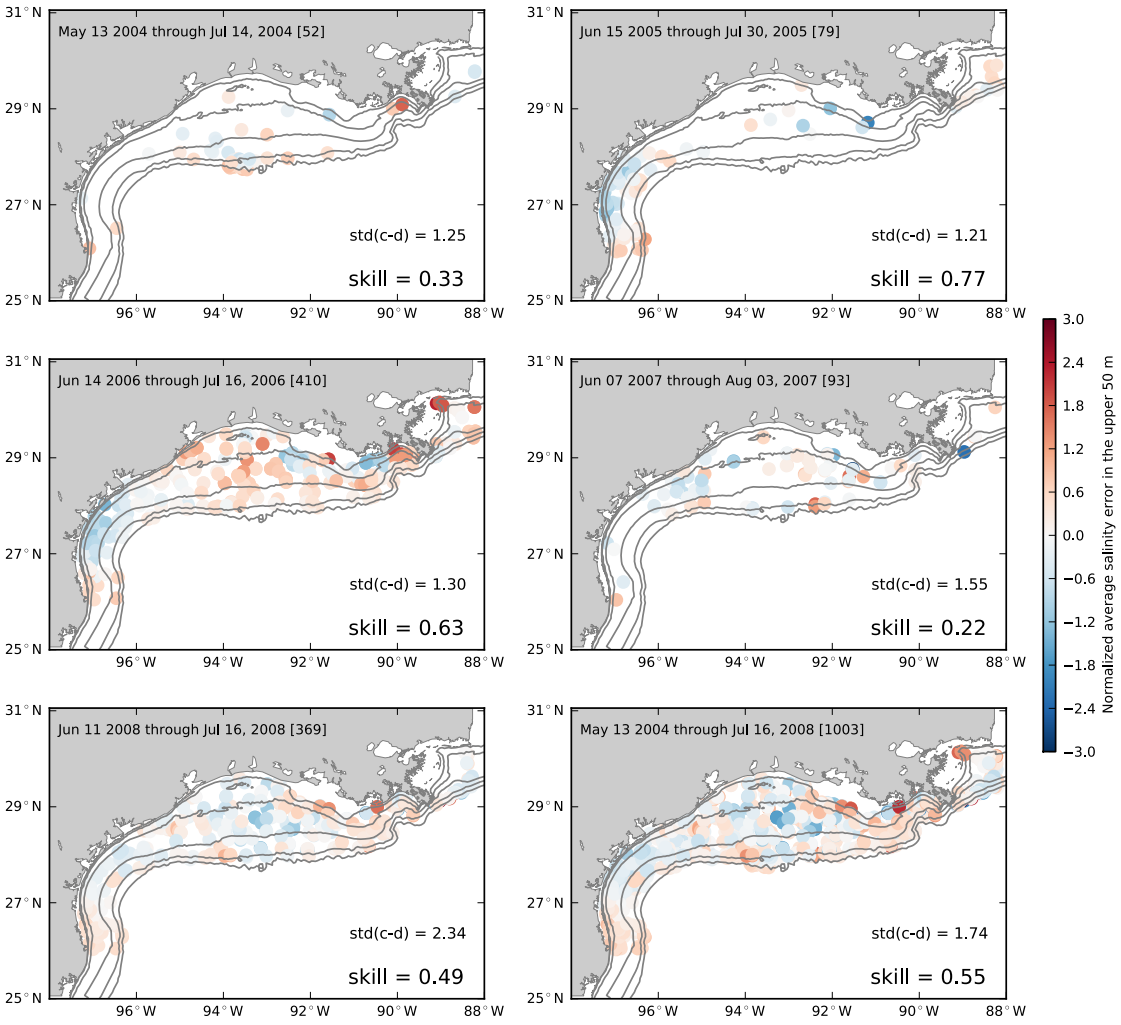

Figure 7. Errors between the model simulated salinity and the SEAMAP measurements averaged over the upper 50 m of water column and normalized by the standard deviation of the difference between the SEAMAP measurements and climatological values for five SEAMAP data collection periods show the spatial patterns of model error for this set of hydrographic measurements. The bottom right panel shows the statistics for all data collected during these periods. The standard deviation of the difference between the observed and climatological values and model skill are provided for each panel.

The second dataset used for assessment is from the Mechanisms Controlling Hypoxia (MCH) project. MCH collected vertical profiles of salinity, temperature and dissolved oxygen concentration data from March to August for year 2004 through 2008 except

2006 [*DiMarco et al.*, 2010]. A total of 1346 profiles are employed in the model-data comparison, as shown in Figure 8, and again, only salinity data in the upper 50 m of the water column are used for computing model errors and skills. For most of the MCH measurement periods the model skill is higher than 0.5, and the highest value is 0.78.

Therefore, it is concluded that the model is able to simulate the observed salinity field reasonably well. Thus, it is expected that the model is able to produce realistic, broad-scale buoyancy forcing over the shelf associated with the Mississippi-Atchafalaya river plume system. This is important, since it will be demonstrated below that buoyancy forcing influences the location of the convergent flows.

2.2.2.3 Surface elevation simulations

Sea surface elevation simulations are evaluated against measurements from the Texas Coastal Ocean Observation Network (TCOON, http://lighthouse.tamucc.edu/TCOON/HomePage). Observational and modeled surface elevations referenced to their annual mean values are compared at three TCOON stations that are not inside a bay (Bob Hall Pier, Galveston Pleasure Pier and Texas Point, Figure 5) for year 2008 (this year has almost complete data coverage). Results (Figure 9) indicate that the variability of observational elevation is well captured by the model simulation for all the three stations, with positive model skills between 0.46 and 0.65.

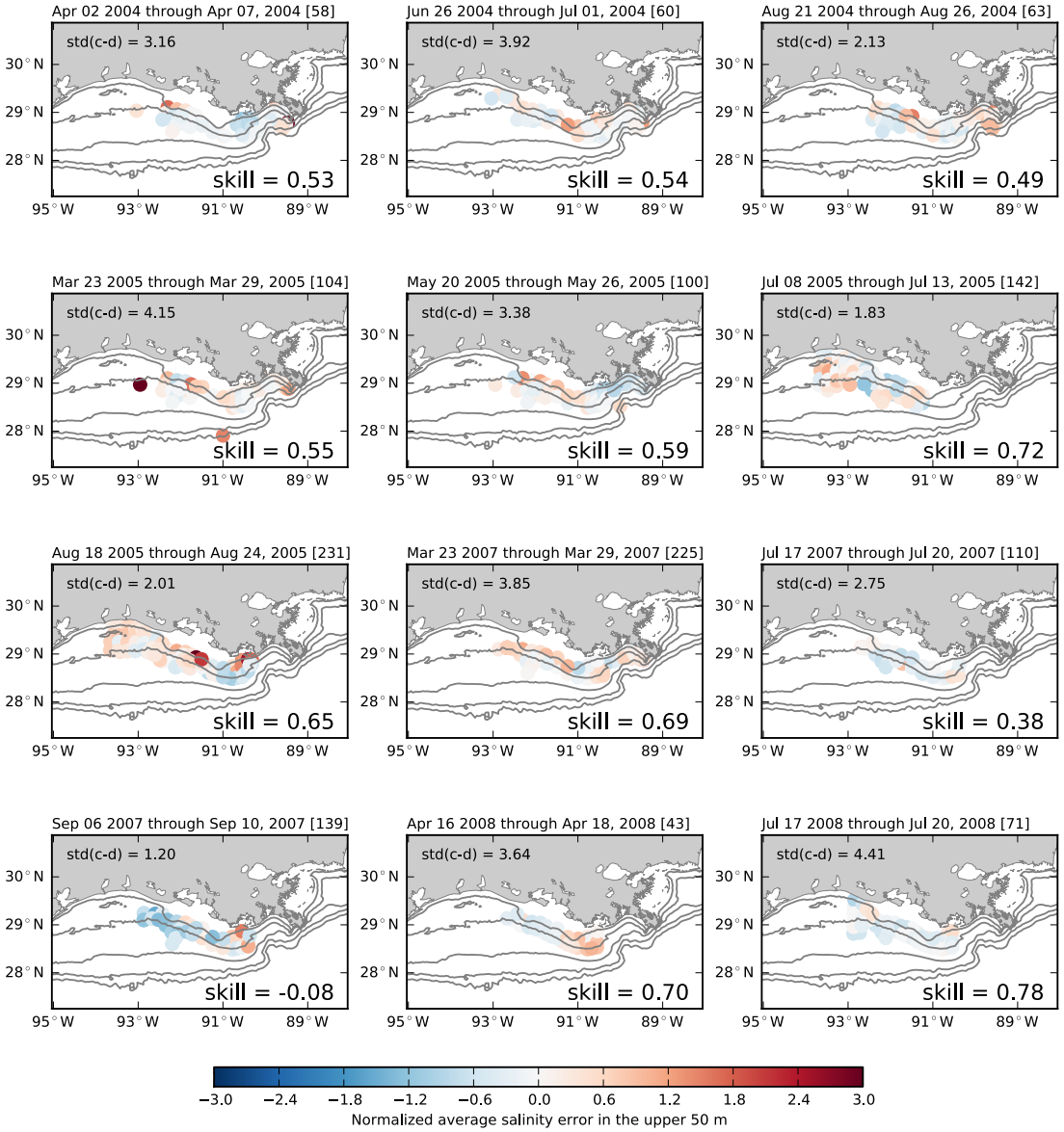

Figure 8. Errors between the model simulated salinity and the MCH measurements averaged over the upper 50 m of water column and normalized by the standard deviation of the difference between the MCH measurements and climatological values for 12 MCH data collection periods show the spatial patterns of model error for this set of hydrographic measurements. The standard deviation of the difference between the observed and climatological values and model skill are provided for each panel.

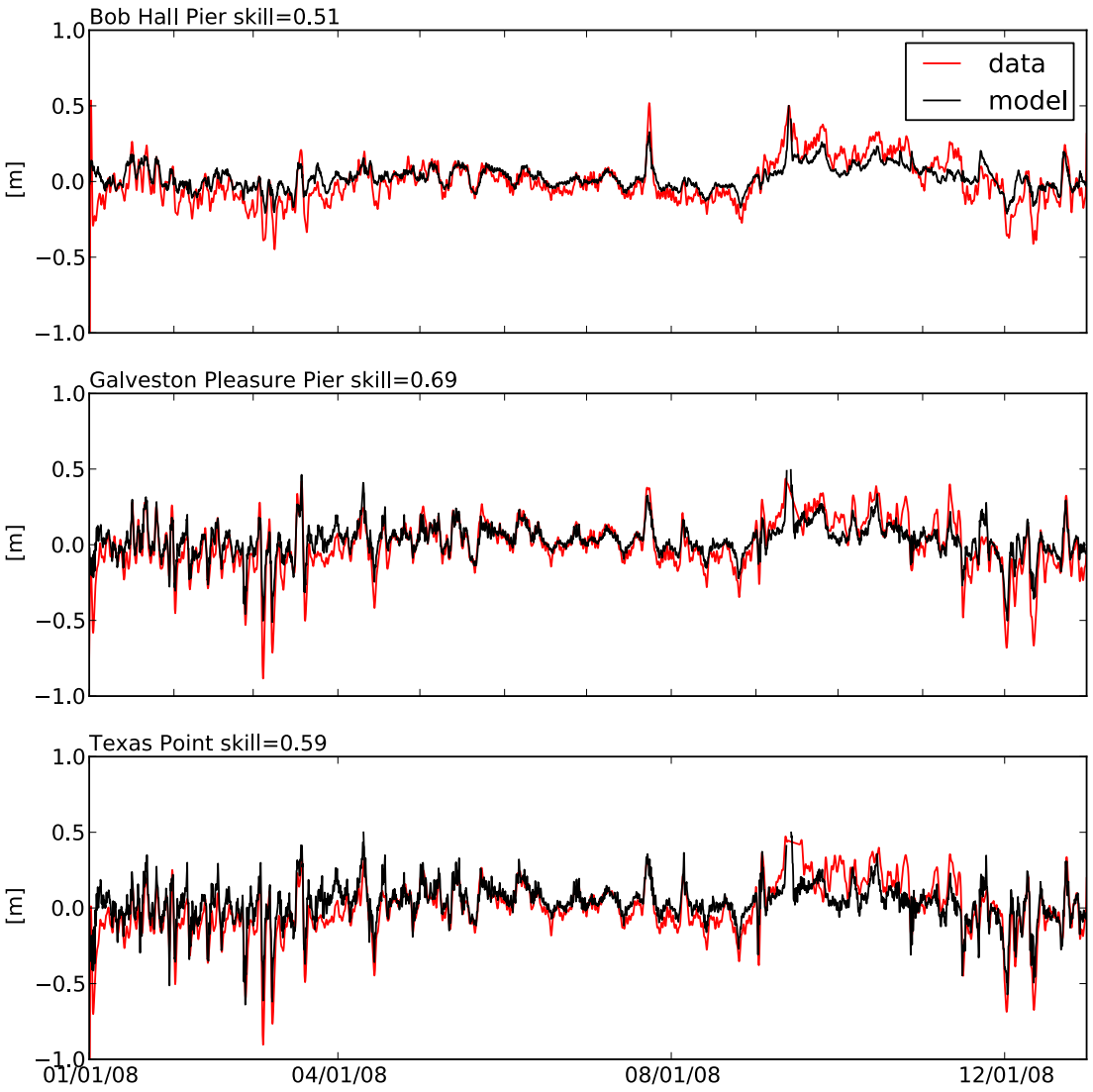

Figure 9. Comparison of the observed (red line) and modeled (black line) sea surface elevations referenced to their corresponding annual mean values at three TCOON stations that are not inside a bay (Bob Hall Pier, Galveston Pleasure Pier and Texas Point, Figure 5) for year 2008.

2.3 Results

Along-shore currents over the Texas-Louisiana shelf undergo a reversal from non-summer to summer months, and the occurrence of convergent flows changes accordingly. In this section, when analyzing the seasonal patterns of convergence, both the non-summer and summer flow regimes are included. However, for weather-band timescales the investigations are mostly focused on the non-summer regime due to the fact that coastal flows in summer are much weaker and less organized because of weaker wind forcing and stronger vertical stratification [*Cho et al.*, 1998; *Jarosz and Murray*, 2005]. Thus, it is more difficult to distinguish convergence events in summer. Model results for year 2006 are used in subsequent analyses since this year shows, overall, better agreement between the simulation and observations, and thus should be a more faithful reproduction of the actual flow field. Winds and currents are both subject to a 33-hr low-band-passing filter to remove near-inertial and higher frequency motions.

2.3.1 Simulated surface convergent flows on the weather band

Figure 10 shows four snapshots of surface flow fields over the Texas-Louisiana shelf when convergent along-shore currents are observed in February 2006, i.e., during non-summer, with surface wind and salinity fields superimposed. From these four examples and other convergent events observed in the model simulation, it is found that convergence mostly occurs near the coast located between Galveston Bay (29.3°N,

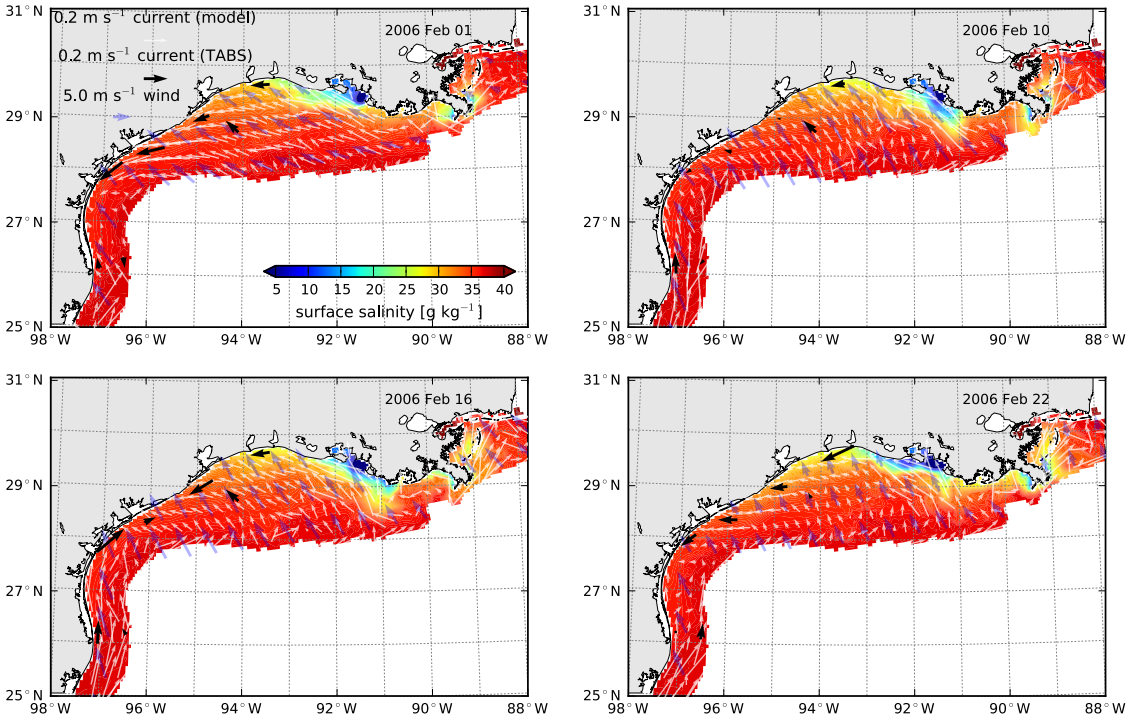

Figure 10. Snapshots of surface current (white arrows), wind (blue arrows), and salinity (color) fields from model simulation and surface currents from the TABS data (black arrows) in February 2006 when convergent flows are observed. Regions deeper than 200 m are masked out because the model does not contain information about deep-water currents, in particular, the Loop Current.

94.8°W) and Baffin Bay (27.2°N, 97.5°W) of Texas. This is the transition zone of the shelf from the north-south orientation in south Texas to the east-west orientation in east Texas and Louisiana. Surface winds over the shelf are quite uniform in direction and generally blow toward the coast (southeasterlies). Although the horizontal variation of wind direction is small, the curvature of the coastline creates dramatic differences in the along-shore component of wind (this is more clearly shown in Figure 12, as will be discussed below), as suggested by *Cochrane and Kelly* [1986]. Along-shore winds are up-coast over the south Texas shelf and down-coast over the Louisiana shelf.

Correspondingly the wind-driven along-shore currents flow in opposing directions in the transition zone and convergence occurs as a result. When northeasterlies prevail over the shelf, along-shore currents are consistently down-coast over the entire shelf, and no convergence is observed. The TABS observations also show the existence of convergent flows at the snapshots in Figure 10, and the model simulated convergence locations are basically consistent with those revealed from observations for 1, 10 and 22 February. For 16 February, the simulated convergence point is located down-coast of the observed convergence location.

Typically, a convergence event can last for several hours up to 2-3 days, depending on the duration of the wind blowing toward the coast. In wintertime, cold frontal passages occur frequently and they usually drive intensified down-coast flows over the Texas-Louisiana shelf [*Nowlin et al.*, 2005], which destroys the convergence events. Figure 11 shows the temporal evolution of a convergence event from 16 to 19 February 2006 and how it is terminated by a frontal passage. Convergent flows are well developed at 00:00 of 16 February near the coast at about 28°N (Figure 11, (a)). The convergence maintains its location at 12:00 of 16 February (b) and moves slightly down-coast at 00:00 of 17 February (c). At 12:00 of 17 February (d), the coastward wind has a dramatic decrease in strength and is more aligned toward the west. With the change of wind the convergence location moves down-coast to 27°N. At 00:00 of 18 February (e), down-coast wind prevails over most of the shelf except for the southernmost section, and the convergence location moves further down-coast to 26°N. The entire shelf is dominated by down-coast

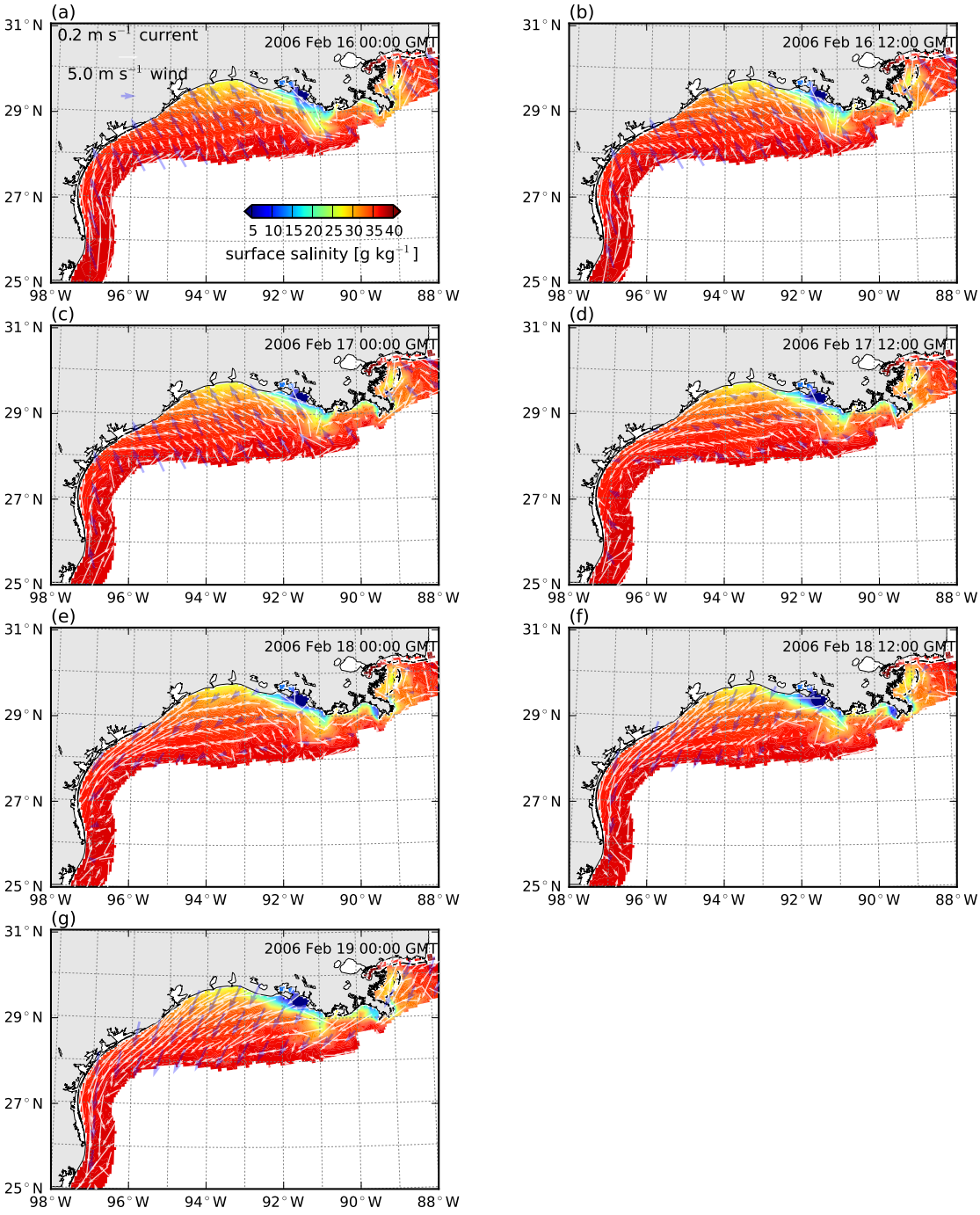

Figure 11. A time sequence of surface current (white arrows), wind (blue arrows), and salinity (color) fields from the model show the temporal evolution of a convergence event and how it is terminated by the passage of a cold front in wintertime. The time interval between consecutive snapshots is 12 h. Regions deeper than 200 m are masked out.

wind at 12:00 of 18 February (f) and the wind strengthens until 00:00 of 19 February (g). Down-coast currents form over the entire extent of the shelf and the convergence phenomenon disappears.

2.3.2 Spatial relation between the convergence in current and wind

To better show along-coast variations in the along-shore wind and current, as well as the location of convergence, a series of cross-shore transects are defined along the Texas-Louisiana coastline. They are placed all the way from the south Texas coast to the central Louisiana coast near the Atchafalaya River mouth (Figure 5). These transects extend from the coastline offshore to the 30-m isobath. Wind and current values on the model grid are interpolated onto points on these transects and the along-shore components are computed for each point, and then the average value over all the points of a transect is used to represent the value of this transect. Figure 12 presents the along-coast distribution of along-shore wind and currents from four times in February 2006 corresponding to the snapshots in Figure 10. We see that, from the south Texas coast to the Louisiana coast, both the along-shore wind and surface currents change from the up-coast (positive) to down-coast (negative) direction; the zero-crossing points are the locations where convergence occurs. The convergence locations of the currents do not overlap those of the wind, but current convergence locations are shifted down the coast relative to the wind convergence locations, i.e. at the zero-crossing point of along-shore wind, there is still down-coast current, while at the zero-crossing point of along-shore

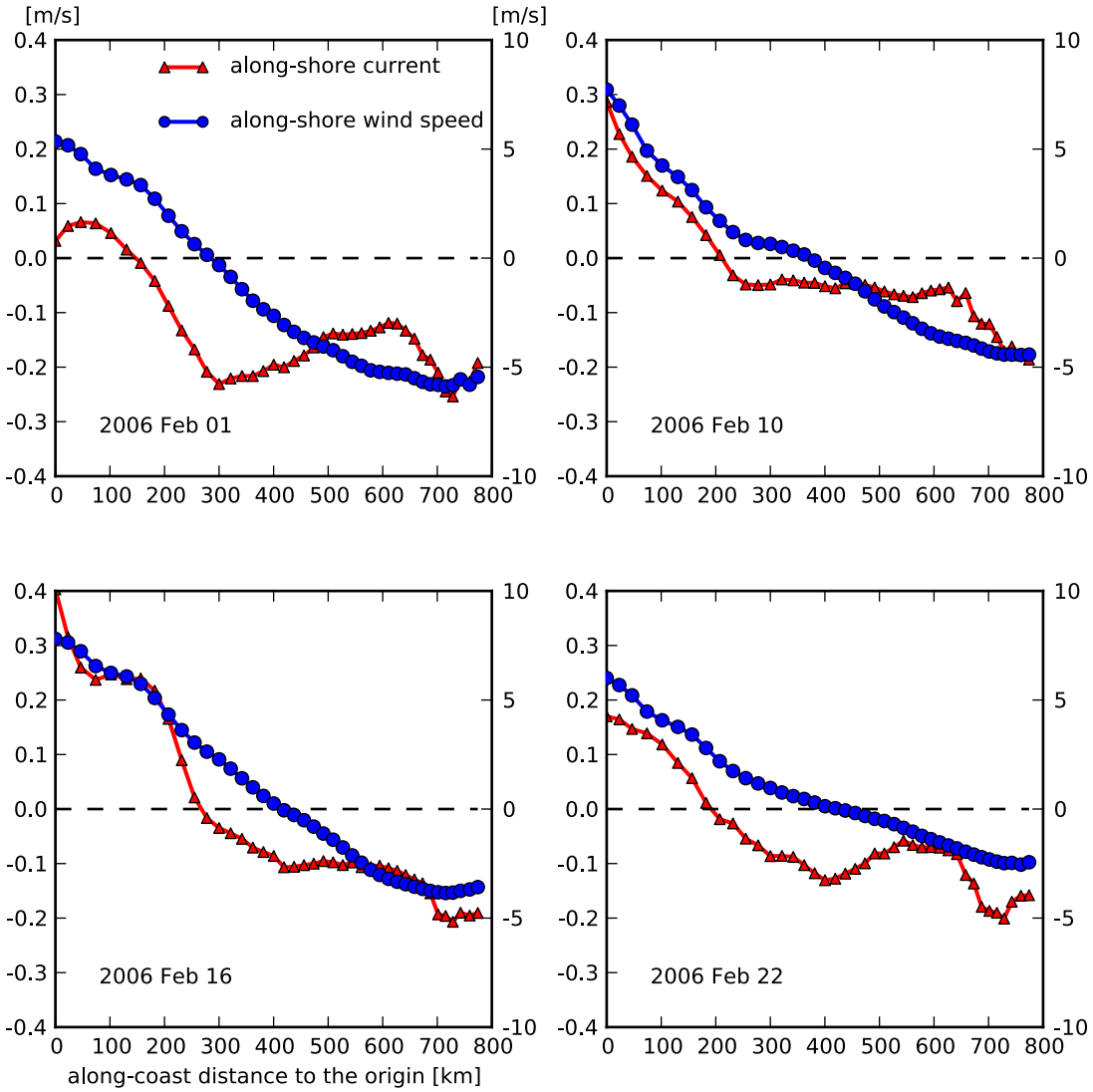

Figure 12. The along-coast distributions of along-shore wind (blue line, right axis) and along-shore surface currents (red line, left axis) are computed from the cross-shore transects (Figure 5) for the same time periods as the snapshots in Figure 10. Positive values denote up-coast-directed winds or currents, and negative values indicate the down-coast direction. The zero-crossing point of each curve is the location where convergence occurs.

current, the along-shore wind is up-coast. The offset between the convergence locations of currents and wind is between 100 and 200 km. The non-wind-driven flow can be roughly estimated by the value of down-coast current at the location of zero wind

forcing in Figure 10, and for the four snapshots the estimates are 0.21 m s^{-1}, 0.04 m s^{-1}, 0.1 m s^{-1} and 0.12 m s^{-1}, respectively.

This shift in the convergence locations of currents from wind indicates that there are other factors that can drive down-coast flow besides wind forcing. One likely factor is buoyancy forcing associated with the Mississippi-Atchafalaya river plume. As discussed in Chapter I, the cross-shore density gradient set up by the plume, which is positive offshore, can drive a down-coast flow. Another factor could be continental shelf waves that propagate information from the east down the coast and introduce non-locally-forced currents. Wind forcing is integrated following a characteristic for a particular shelf wave mode, so a particular shelf wave mode carries the memory of previous wind conditions [*Gill and Schumann*, 1974]. This, too, would tend to shift the convergence point of currents down-coast. As currents in up-coast locations are always associated with down-coast flow, shelf waves will tend to carry the memory of this down-coast, wind-forced flow further down the coast. Continental shelf waves on the Texas-Louisiana shelf have been observed by *Nowlin et al.* [1998].

2.3.3 Wind influence

To further study the relation between surface along-shore current and wind speed, scatter plots are made for the two variables for three winter months: January, February and March of 2006 (Figure 13a). Strong correlation between current and wind speed has

been observed in many previous studies; for example, *Whitney and Garvine* [2005] used this relation to estimate wind influence on the Delaware coastal currents. The plots in Figure 13a reveal a positive correlation between surface current and wind speed, with $r^2 > 0.75$ for all transects except those located between the 200-km and 400-km location. This is the zone where convergence frequently occurs, and, as discussed above, the along-shore current is not quite in phase with the local along-shore wind at convergence locations, thereby reducing the correlation somewhat. There is clearly a hysteresis in the lagged response of currents to the wind that causes the cloud of points to spread to an oval shape, instead of an exact linear relationship. However, there is also clearly a shift in the correlation toward the fourth quadrant, with down-coast currents under up-coast winds occurring more often than the opposite case. This suggests that there is a mean down-coast flow during times of convergence similar to that expected for buoyancy forcing or continental shelf waves. The magnitude of this flow can be estimated by the y-axis intercept, which denotes current under zero wind forcing. For all of the transects the y-axis intercept values are negative, meaning that there are down-coast currents when wind forcing disappears. The non-wind-driven down-coast current is strongest at the 300-km and 400-km transects and approximately 0.07 m s^{-1}, slightly lower but roughly the same magnitude as the four examples shown in Figure 10.

Figure 14 displays the time lag correlation between the along-shore current and wind speed for the transects shown in Figure 13. In wintertime, the two variables have very high correlation (over 0.8 for most of the transects) at time lag 0, and the highest

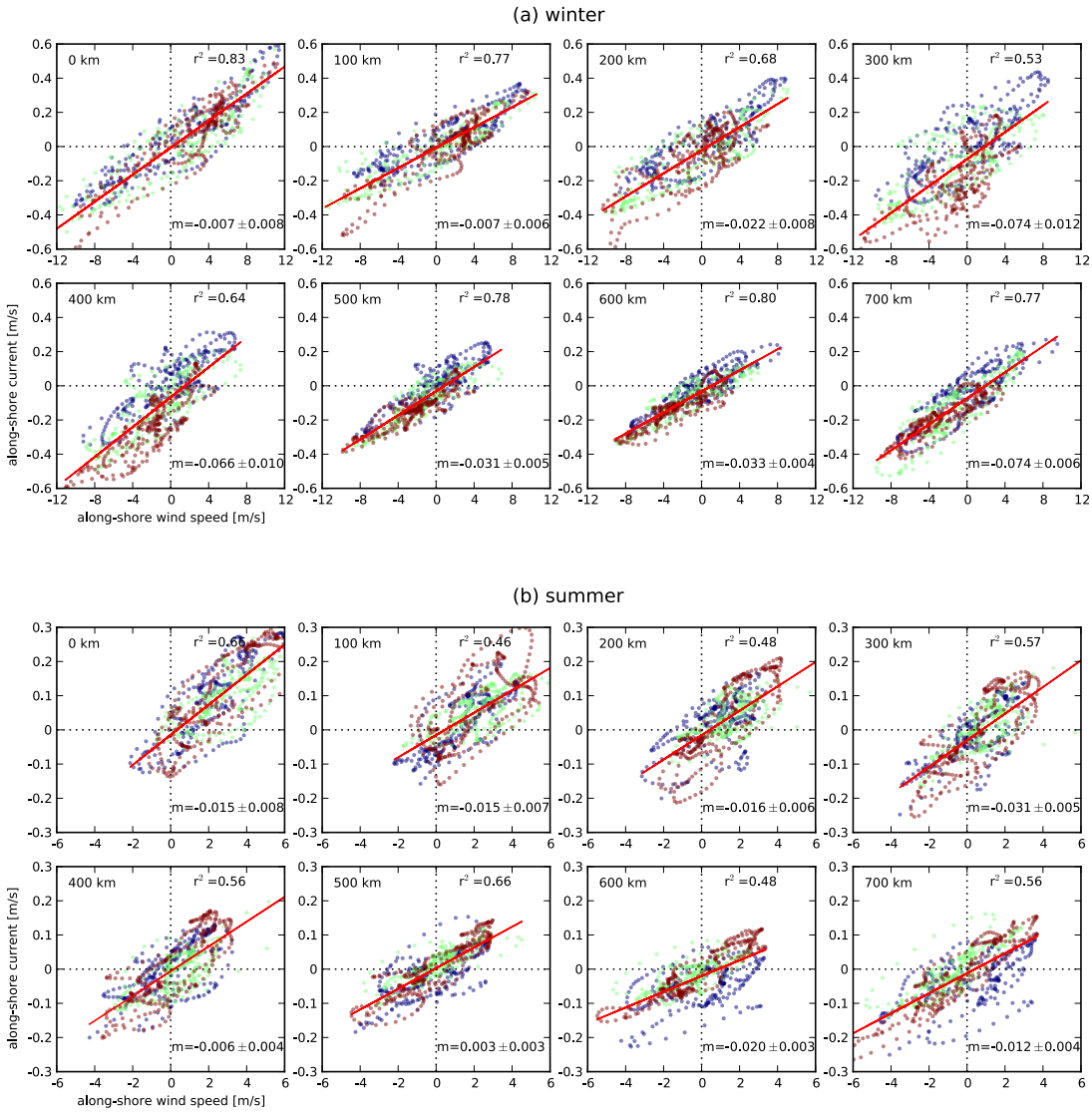

Figure 13. Scatterplots of 3-hourly surface along-shore current versus along-shore wind speed for the 0, 100, 200, 300, 400, 500, 600, and 700-km transects shown for (a) three winter months (January (purple dots), February (green dots), and March (maroon dots)) and (b) three summer months (June (purple dots), July (green dots), and August (maroon dots)) of 2006. Linear regression is performed for each plot, and the corresponding r2 value is provided. Also provided is the y intercept value (m) of the regression line (red) at the 95% confidence level.

correlation occurs when surface currents lag behind wind for 3 hours. After 3 hours, the correlation coefficient shows exponential decay within the time lag of 48 hours except

for the 300-km and 400-km transects, and the e-folding timescale is between 20 and 60 hours. For the 300-km and 400-km transects, the correlation coefficient also decays with time but with a linear pattern. Therefore compared to other transects, currents at these two transects have stronger inertia. In general, the analysis of along-shore wind and surface along-shore currents in winter reveals a fast response of currents to wind on the weather band.

In summer months, winds are weak and currents become sluggish (Figure 13b; note that both the range of x-axis and y-axis are just half of that in winter), and the correlation between surface currents and wind shows a slight reduction. Instead of near-instantaneous response to the wind forcing as in winter, the currents display more inertia, in that the highest correlation between currents and wind occurs at a longer time lag, e.g. ~12 hours for transects south of the 300-km location. Also, there is a weaker decay of the correlation with increasing time lag. The long time lag may be a consequence of relatively weak wind forcing. However, prominent convergent flows are also observed in summertime under strong wind conditions, and their characteristics are similar to those in winter. As mentioned above, the more disorganized currents in summer generally render the convergence pattern more complex than in winter, and the long correlation time lag may play an important role in this.

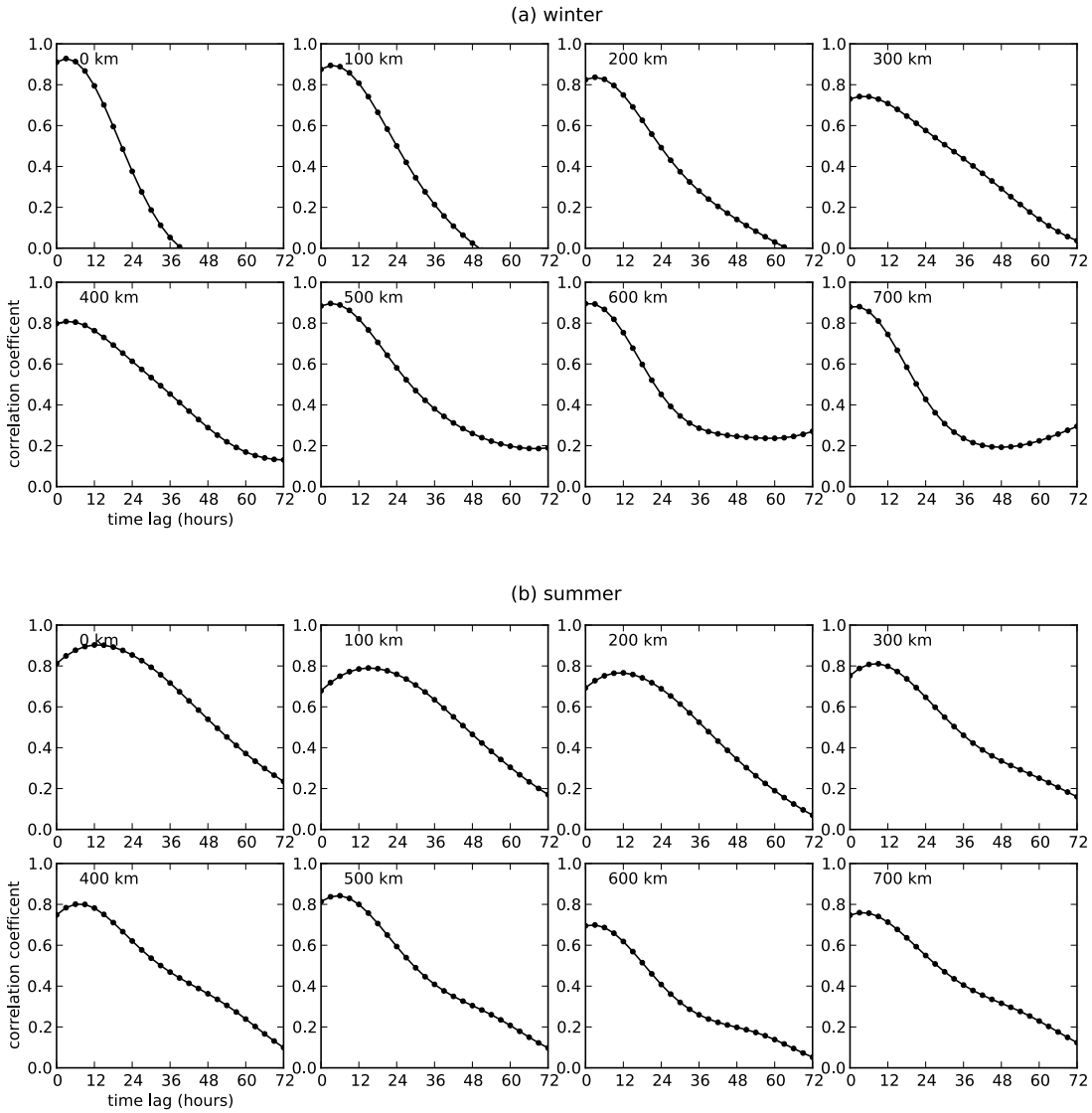

Figure 14. Time lag correlations between 3-hourly surface along-shore current and along-shore wind speed for the cross-shore transects in Figure 8 show that currents lag wind forcing by 3 to 12 h.

2.3.4 Buoyancy influence

Buoyancy forcing resulting from the Mississippi-Atchafalaya river plume drives the along-shore current through a thermal wind balance, that is,

$$u_z = \frac{g}{\rho_0 f}\frac{\partial \rho}{\partial y}\ , \tag{2}$$

where u is the along-shore velocity, g is the gravitational acceleration, f is the Coriolis parameter and ρ_0 is the reference density; the subscripts z and y denote vertical and cross-shore gradients, respectively. Figure 15 presents the cross-sectional profiles of mean salinity, temperature and density over January, February and March of 2006 along a cross-shore transect in the region where convergence usually happens (this section is approximately at the 300-km location). Salinity (Figure 15, (a)) increases in the offshore direction as a result of fresh water introduced at the coast, and the isohalines are fairly vertically aligned as a result of down-coast wind straining, which was discussed in 1.1.1.2. The horizontal gradient of salinity is slightly larger inshore of the 40-m isobath than offshore. The plume on the whole displays a pattern that is similar to the 'bottom-advected plume' described by *Chapman and Lentz* [1994] and *Yankovsky and Chapman* [1997], but with a much wider density front. Such plume pattern will be discussed in detail in Chapter III. Temperature (b) also increases offshore, attributed to the distribution of solar radiation, greater cooling of the shallow coastal water under wintertime surface heat loss and the presence of cold plume water along the coast. Salinity is the major determinant of density, and the isopycnals (c) also have a stronger

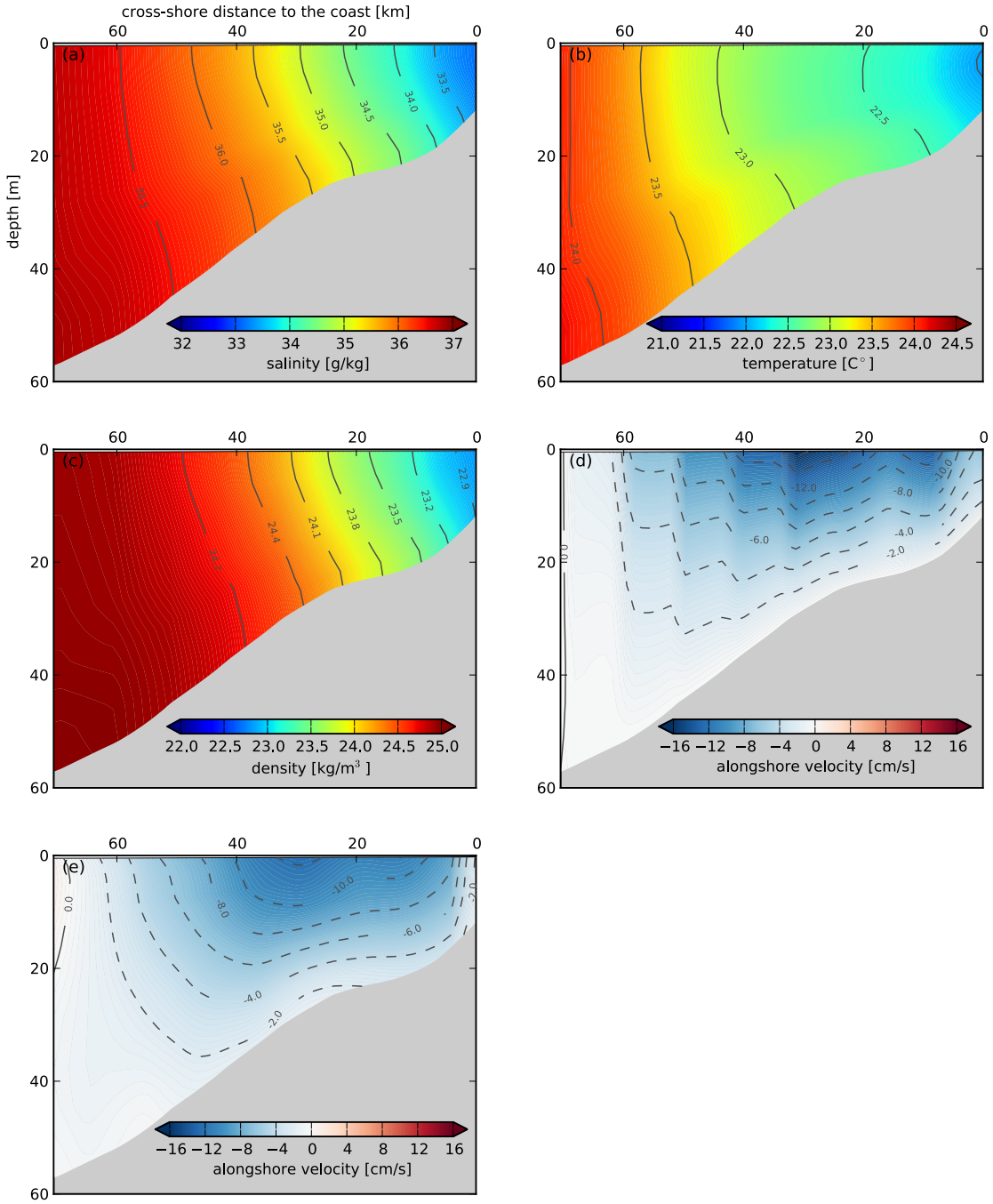

Figure 15. Vertical - cross-shore sections of (a) mean salinity, (b) temperature, (c) density, (d) along-shore velocity derived from the thermal wind balance and (e) along-shore velocity from model results over January, February and March of 2006 for a cross-shore transect near 28°N.

gradient inshore of the 40-m isobath; the highest horizontal gradient occurs in the area between the 25-m and 35-m isobath. Using this density profile, the along-shore velocity at each depth level is computed by vertically integrating equation 2 and assuming a zero bottom velocity, as in *Yankovsky and Chapman* [1997]. The rationale of using this method to estimate the buoyancy-driven along-shore flow will be explained in Chapter III. The resulting profile of along-shore current is shown in Figure 15 (d). The result suggests that buoyancy can induce down-coast currents of approximately 0.12 m s^{-1} near the surface. In the high density gradient region between the 25-m and 35-m isobaths the largest along-shore surface current is ~ 0.14 m s^{-1}. Averaging the surface along-shore velocity over the span from the coastline to the 30-m isobath yields a value of 0.12 m s^{-1}. This number is larger than the estimated buoyancy-driven current for the 300-km transect (~ 0.07 m s^{-1}) in Figure 13. The reason for the overestimate could be that the buoyancy-driven current in Figure 15 is estimated by a density profile forced by down-coast wind (mean wind stress over January, February and March is down-coast). As will be discussed in Chapter III, such wind would create a bottom-advected plume pattern in which the buoyancy-driven flow can play a larger role in the along-shore flow dynamics than that in a no-wind environment (Figure 13). However, the value of 0.12 m s^{-1} can still provide a rough estimate of buoyancy-driven currents without wind forcing, and it falls into the range of the estimated non-wind-driven down-coast currents from the four examples in Figure 10. This could be an indication that buoyancy forcing contributes to most of the non-wind-driven currents and thus the offset between convergent currents and winds. The profile for model-produced mean along-shore flow over January,

February and March of 2006 is presented in Figure 15 (e). The mean flow field shows overall a baroclinic structure that is similar to the buoyancy-driven flow field (Figure 15 (d)). This suggests that the thermal wind balance is a good approximation of the along-shore flow dynamics on seasonal scale in the non-summer flow regime. This point will be confirmed in Chapter III, which includes a more thorough analysis of how much the thermal-wind-balance-derived flow can account for the actual along-shore flow in non-summer.

A sensitivity model run with the Mississippi-Atchafalaya river discharge removed is conducted, as a way to test the effect of buoyancy on the convergence. The locations of convergent surface currents and winds for the same snapshots in Figure 10 are shown in Figure 16, but for the case with no river discharge. Without buoyancy forcing, convergence still occurs at these times, confirming that wind is the determining factor for the formation of convergent flows. However, there is a marked shift in the location of convergent currents compared to that in Figure 12, such that the convergent flows now occur very close to the locations of convergent winds. This, again, suggests that buoyancy forcing is the primary factor leading to the offset between the convergent currents and winds. For 10 February, the down-coast drift of convergent currents from winds are still observed, implying that besides buoyancy forcing, continental shelf waves may also play a role in forcing down-coast currents. A detailed analysis of the effect of continental shelf waves is beyond the scope of this study, but a brief discussion on its impact on the convergence location will be provided in 2.4.

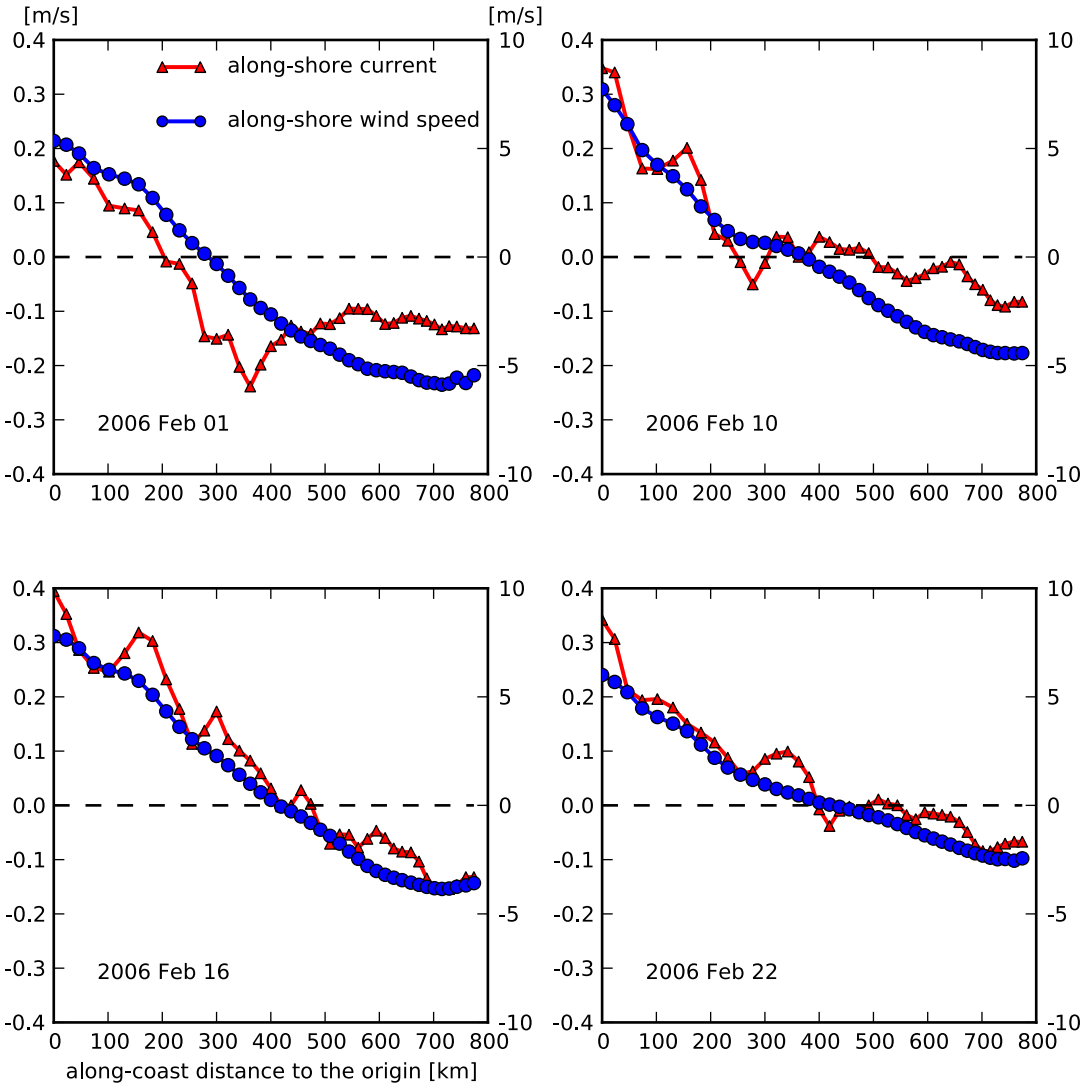

Figure 16. Same as Figure 12 but for the sensitivity run in which river discharge is taken out.

2.3.5 Temporal variation of convergent along-shore flows

2.3.5.1 Weather-band pattern

As wind over the Texas-Louisiana shelf is highly variable in non-summer over timescales of roughly 3-10 days [*Wang et al.*, 1998], , the weather-band, it is expected that convergence of wind, as well as currents, also have strong temporal variations. Figure 17 displays the along-coast distribution of 3-hourly along-shore wind (left panel) and surface currents (right panel) varying with time in winter and spring of 2006. No band-passing filtering is applied to the 3-hourly data. A fourth-order polynomial function is fit to the spatial distribution curve for each time moment to find out the convergence location where along-shore values change from up-coast (positive, red color) to down-coast (negative, blue color). We see that the 3-hourly wind displays a strong variability over time, consistent with the conclusion drawn by *Wang et al.* [1998]. Correspondingly the convergence of wind occurs over a broad range of spatial scales (the black dots are spread over 0-km - 800-km). The along-shore currents make a similar pattern to that of the along-shore wind. Because the timeseries is not filtered, near-inertial motions are clearly seen in the current field as stripped patterns with a cycle of ~1 day. The near-inertial motions are particularly strong between March 15 and May 15. This is because the wind field is gradually dominated by diurnal signals from spring to summer, and as frontal passages are less common, as well as vertical stratification

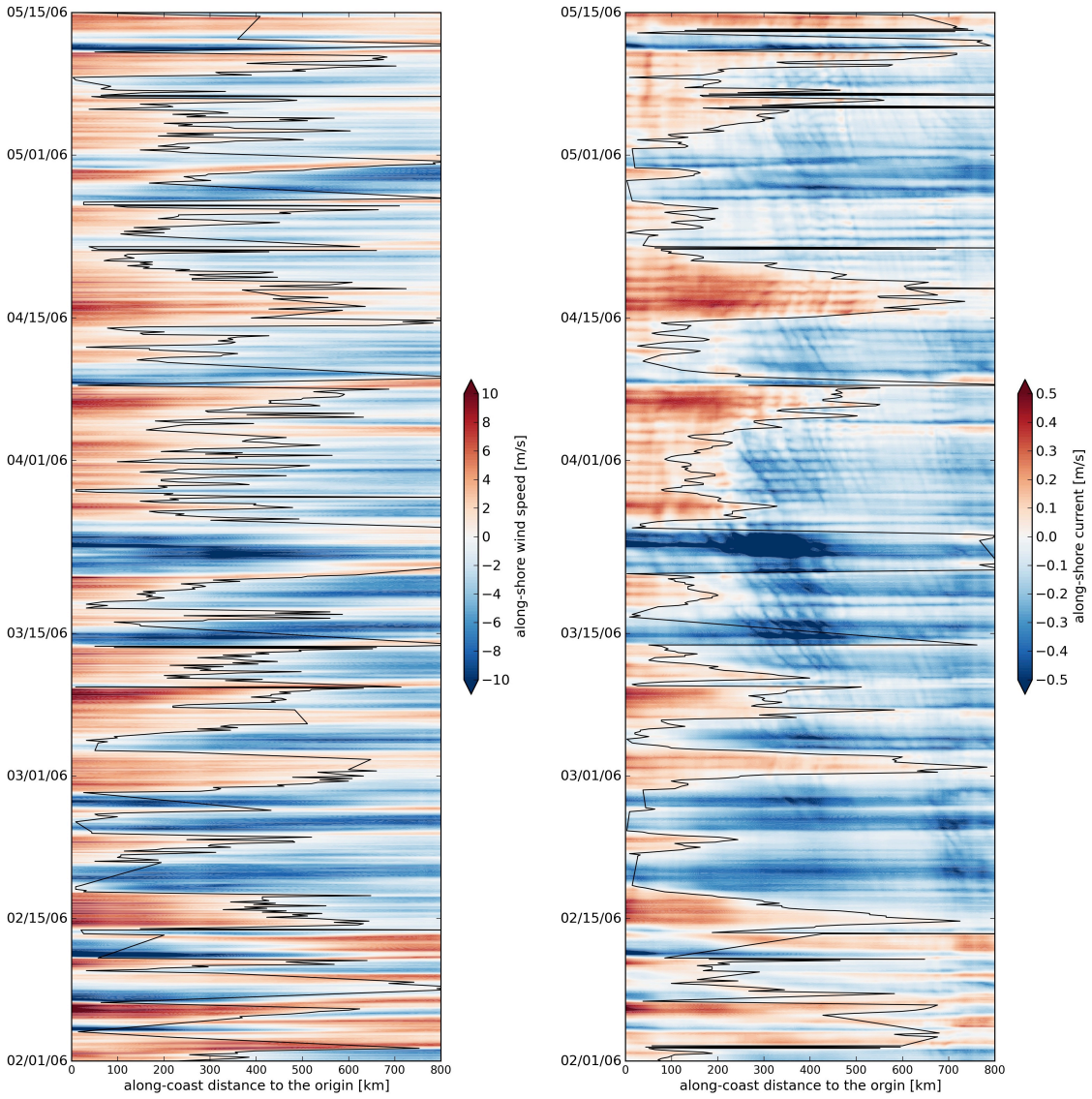

Figure 17. The Hovmöller diagram of non-filtered 3-hourly (left) along-shore wind speed and (right) along-shore surface current from the model simulation for 2006 winter and spring shows the evolution of along-shore wind and currents in time. The x axis is the along-coast distance to the origin, and the y axis is date. Up-coast values are positive and represented by red colors, and down-coast values are negative and represented by blue colors. The black line in each plot connects the convergence points at different times. The convergence point for each time moment is found out by fitting a fourth-order polynomial function to the spatial distribution curve for wind and current at this moment and then locating the zero-crossing point of the polynomial function.

strengthens, more inertial-band energy is trapped in the surface layer [*Zhang et al.*, 2009; *Zhang et al.*, 2010]. The convergence point of currents is also spread over a wide range, but its variability is not as high as that of wind. Most of the convergent currents occur between the 100-km and 500-km locations, and these locations are generally down the coast of the wind convergence points. For the weather-band convergence, no specific character is found in its temporal variation.

2.3.5.2 Monthly mean pattern

Seasonal-scale convergence has been mentioned in several studies, but very few have analyzed its temporal variation. Only *Morey et al.* [2005] suggested that there is a seasonal migration of monthly convergence location along the coast. Here a more thorough discussion will be provided for the seasonal variation of monthly convergence pattern. Compared with *Morey et al.* [2005] that uses monthly climatological wind forcing in their model, this study uses the real-time wind forcing, allowing us to investigate the interannual variability of monthly convergence. Figure 18 (left) shows the along-coast distribution of monthly mean along-shore wind and surface currents varying with month in 2006. The monthly mean convergence displays a prominent seasonal pattern. The convergence of wind generally migrates up-coast in spring and summer, with an exception due to anomalous winds in January with anomalous weak down-coast winds over the northern shelf opposed by anomalous strong up-coast winds

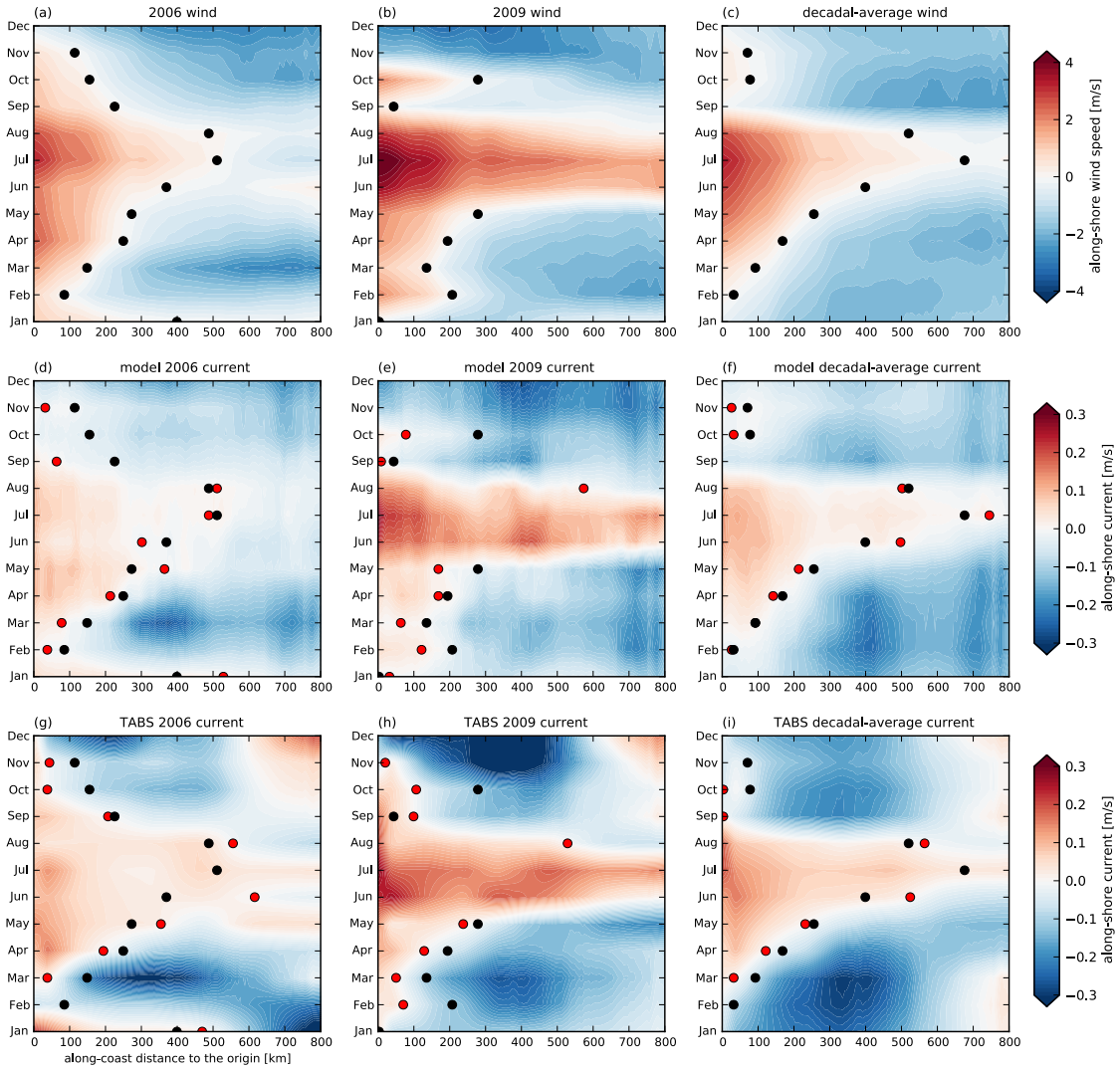

Figure 18. The Hovmöller diagrams of monthly mean (a–c) along-shore wind speed, (d–f) along-shore surface current from the model simulation, and (g–i) along-shore surface current from the TABS buoys for the year (left) 2006, (middle) 2009, and (right) 10-year average show that there is significant seasonal and interannual variability in the convergence locations for currents and wind. The x axis is the along-coast distance to the origin, and the y axis is month. Up-coast values are positive and represented by red colors, and down-coast values are negative and represented by blue colors. The black dots mark the convergence points for wind, and the red dots mark the convergence points for currents.

from south, shifting the convergence point further up-coast relative to the locations in normal winter months. As down-coast winds strengthen in February, the convergence

point of wind retreats back to the 100-km location, and with the development of up-coast winds and their intrusion toward the upper coast in spring and summer, convergence marches up-coast all the way to the 500-km location in July. Thereafter, down-coast winds begin to gain strength and their down-coast intrusion forces the convergence location to retreat all the way down-coast until November. In December, the study area is dominated by down-coast winds and no convergence is observed. The evolution of convergent currents bears close resemblance to the wind pattern, but in October convergent flows are not obviously seen, and they might have moved further down-coast to the east Mexico shelf - an area that is included in the studies of *Morey et al.* [2005] and *Zavala-Hidalgo et al.* [2003]. A comparison between the locations of convergent currents and winds shows that for most months (February, March, April, June, July, September and November), convergent currents occur down-coast of convergent winds, but the offset is generally less than 100 km, smaller than the snapshot values (Figure 12). A possible reason is that, on seasonal scales, the effects of weather-band dynamical features (like shelf waves) on currents decrease, resulting in more consistent flow and wind patterns.

The seasonal pattern of monthly mean convergence has interannual variability. Figure 18 also presents the convergent winds and currents in 2009 (middle), which is notable for its anomalously strong up-coast winds in summer. We see that in the summer months, up-coast winds have greater strength than those in 2006, and they also reach much farther up-coast so that convergence of wind does not occur in the study region. The

marching of convergence of currents basically follows that of wind in spring (February to May) and fall (September and October), and in June and July no convergent currents are observed.

Seasonal variation of convergence based on a ten-year (2001-2010) average is shown in Figure 18 (right). The average decadal pattern shows that convergence initially develops in February within the study region. The up-coast migration of convergence from spring to summer and down-coast retreat in fall and winter is similar to the 2006 case, while in summer months the convergence location reaches further up-coast relative to 2006, as a result of greater intrusion of up-coast winds. But this intrusion is not as strong as in 2009, and convergence of wind and currents can still be observed in the study area.

The monthly mean pattern of convergence using the TABS data is also investigated and provided in Figure 18g-i. These data are sparsely distributed in space and cannot resolve the convergence locations exactly, but it is anticipated that a seasonal pattern may be revealed by the observations as well. Only data from the inner-shelf buoys are used, since dynamics of the outer shelf are different from those of the inner shelf, and including the offshore buoy data can bias the results. Surface velocity data from buoys B, D, F, J, K, R and W are interpolated onto the cross-shore transects and rotated to the along-shore direction. Results of the monthly mean convergence are shown in Figure 18g-i. As expected, in spite of their low spatial resolution, the TABS data still reflect a

seasonal variation in the convergence location, very similar to that calculated from the numerical simulation.

2.4 Discussion

The local response of along-shore currents to along-shore wind can be investigated by a barotropic friction model. The slope burger number, defined as $\alpha^2 N^2/f^2$ [*Clarke and Brink*, 1985], is <<1 for most of the Texas-Louisiana shelf in the winter seasons (based on computations using the ROMS model and hydrographic observations), where α is the average shelf bottom slope and N^2 the buoyancy frequency. This suggests that a barotropic model is appropriate for describing the shelf dynamics [*Clarke and Brink*, 1985; *Lentz*, 2008] on the Texas-Louisiana shelf, while *Jarosz and Murray* [2005] also demonstrated that in wintertime there is a predominant barotropic response of the inner shelf currents to strong winds. The depth-averaged along-shore momentum equation is written as

$$\frac{\partial u}{\partial t} - fv = -g\frac{\partial \eta}{\partial x} + \frac{F^x}{H} - \frac{ru}{H}, \tag{3}$$

where u is the depth-averaged along-shore velocity, v is the depth-averaged cross-shore velocity, η is the surface elevation, F is the kinematic along-shore wind stress, r is a linear bottom drag coefficient and H is the water depth. The bottom friction term acts as an energy sink, and equating the scales of this term and the local acceleration term gives a frictional spindown timescale of

$$T = H / r \,. \tag{4}$$

If we take the linear bottom drag coefficient r as 3×10^{-4} m s^{-1} for the Texas-Louisiana shelf following *Jarosz and Murray* [2005], and an average depth of 15 m inshore of the 30-m isobath, a decay time of 14 hours is obtained. The magnitude of this value is roughly the same as that of the decay scale derived from the lag correlation analysis in 2.3.3. Discrepancies could arise from baroclinic factors that are not represented in this barotropic friction model.

The model results suggest that the offset between the wind and current convergence points cannot always be explained entirely by buoyancy forcing, although buoyancy forcing does appear to be the dominant factor in creating this offset. Continental shelf waves are most likely responsible for the remaining balance, and for long timescales in shallow water where bottom friction may be an important factor, the residual flow caused by shelf waves may be explained by arrested topographic wave theory [*Csanady*, 1978]. This study does not aim to quantitatively compute the magnitude of the flow caused by shelf waves, since that would require detailed knowledge of the wind forcing along the coast and is outside the scope of the analysis. Rather, the distance of a persistent wind source influencing the local current regime is estimated by the along-shore decay scale of the topographic waves. The governing equation for such waves is

$$\frac{\partial^2 \eta}{\partial y^2} + \frac{f}{r}\frac{dh}{dy}\frac{\partial \eta}{\partial x} = 0 \,, \tag{5}$$

where η is the surface elevation and h is the water depth; x and y denote the along-shore and cross-shore directions respectively, with positive x pointing down-coast and positive y pointing offshore [*Csanady*, 1978]. If we use X, Y and H to denote the along-shore, cross-shore and vertical scales, respectively, then the first term on the l.h.s of equation 5 can be scaled as H/Y^2, and the second term scaled as fH^2/rXY. Equating these two scales yields

$$X \sim \frac{fHY}{r}. \tag{6}$$

Using the same values for r and H as in equation 4, and assuming a cross-shore scale Y of 50 km, with an average Coriolis parameter of 7×10^{-5} s^{-1}, an along-shore spatial decay scale of $X \sim$170 km is obtained. This means that currents in one region can be influenced by wind forcing from as far as 170 km up-coast of this region. This scale is the same order as the spatial offset of the wind and current convergence points, and so it is concluded that shelf waves could have an influence on shifting the convergence point of currents down-coast.

Eliminating the river forcing could also have a nonlinear influence on other dynamical aspects, such as the response of currents to local winds and shelf waves, or changes in bottom drag. The offshore density gradient tends to establish a thermal-wind-balanced vertical shear that reduces the along-shore velocity near the bottom, thus reducing bottom drag relative to what would be estimated only considering the vertical mean flow. So, once this density gradient is eliminated, the bottom drag may be enhanced,

which in turn leads to a decrease in the spindown timescale, and a faster response of currents to local winds. Also, as bottom drag increases, the along-shore decay scale of shelf waves decreases, and a reduction in the non-local effect of winds might be expected.

Convergence of along-shore currents can be compensated by offshore transport. Such transport has been reported by previous studies on the fresh water transport over the western shelf of the Gulf of Mexico. *Zavala-Hidalgo et al.* [2003] suggested that an offshore transport of at least 0.1 Sv can be generated by the convergence in the Bay of Campeche. *Morey et al.* [2005] found the most vigorous cross-shore export of fresh water occurring during spring and fall in the convergence region of the Texas-Louisiana shelf. A recent study of the Mississippi and Atchafalaya fresh water transport over the Texas-Louisiana shelf by *Zhang et al.* [2012a] observed an up-coast migration of enhanced freshwater outflow from winter to summer (see their Figure 9 and Figure 10), and it is inferred that this is associated with the seasonal migration of the convergent currents.

CHAPTER III

BUOYANCY-DRIVEN SEASONAL ALONG-SHORE FLOW IN THE NON SUMMER FLOW REGIME OF THE TEXAS-LOUISIANA SHELF

3.1 Background

In Chapter II, it has been shown that buoyancy plays a role in driving along-shore currents, and thus can push the location of convergent currents down-coast of the location of convergent winds. In this chapter, the buoyancy forcing effect on the along-shore circulation in non-summer will be investigated more thoroughly. While the along-shore circulation in the study of convergent flows is taken as wind-driven flow influenced by buoyancy forcing, in this chapter, it will be considered from a different perspective, and taken as buoyancy-drive flow influenced by wind. The rational for taking such perspective was given in 1.2.2. This study is the first one to explore the buoyancy-driven circulation under the modulation of seasonal wind on the Texas-Louisiana shelf.

In non-summer, under prevailing down-coast winds, the Mississippi-Atchafalaya fresh water plume was shown in Chapter II (2.3.4) to exhibit a bottom-advected pattern, in which the offshore edge front of the plume can extend from surface to bottom. *Chapman and Lentz* [1994] studied the dynamics of the bottom-advected plume under no wind forcing, and they demonstrated that there is a two-way adjustment between the buoyancy

advection and the along-shore flow. On the one hand, the along-shore flow, which is to the right of the river discharge in the Northern Hemisphere, induces an along-shore stress at bottom; the bottom stress generates an offshore Ekman transport that advects buoyancy off the coast in the bottom boundary layer. On the other hand, the offshore buoyancy advection causes a homogenization of the water column near the coast and pushes the surface-to-bottom density front, which is responsible for a strong vertical shear in the along-shore flow, offshore. An equilibrium state is reached when the front is advected to water deep enough that the vertical shear can reverse the along-shore flow across the base of the front, and the onshore Ekman transport at the front base shuts down the offshore buoyancy advection. The shut down of buoyancy fluxes is also found in a study of bottom boundary layer dynamics on a slope by *MacCready and Rhines* [1993]. It is expected that a situation similar to that described by *Chapman and Lentz* [1994] should occur for the bottom-advected Mississippi-Atchafalaya river plume in non-summer. However, *Chapman and Lentz* [1994] discussed a case without wind forcing; with wind forcing, the plume front can be substantially displaced, and an equilibrium state as shown above can rarely be reached, but a near-equilibrium state may be anticipated for the seasonal-scale circulation. It will be investigated below how the flow dynamics for the wintertime Mississippi-Atchafalaya river plume is similar to or different from the theory of *Chapman and Lentz* [1994].

The theory of *Chapman and Lentz* [1994] on the bottom-advected plume evolution is supported by *Yankovsky and Chapman* [1997]. Considering the facts that the along-shore

flow is in thermal wind balance with the horizontal density gradient in the plume front, and that it is only reversed to a small opposite value at bottom, *Yankovsky and Chapman* [1997] suggested that the along-shore flow in the plume front can be estimated by the thermal wind relation with an assumption of zero bottom flow. This study will use the same method as *Yankovsky and Chapman* [1997] to estimate the thermal-wind-balanced flow, and the major objective is to identify how much this thermal-wind-balanced flow can explain the actual along-shore flow in wintertime. The thermal wind relation and zero-bottom-flow assumption will be applied to the entire shelf, as it will be shown below that in many cases, the density front of the Mississippi-Atchafalaya river plume is quite wide and can span nearly across the shelf.

3.2 Numerical model

The numerical model employed in this study is also based on ROMS. The model grid covers the entire Texas and Louisiana shelf and slope region (Figure 19), with a horizontal spacing of ~ 500 m near the coast and ~ 1-2 km over the outer slope [*Zhang et al.*, 2012a; *Zhang et al.*, 2012b]. The model has 30 terrain-following layers irregularly spaced in the vertical direction, with a minimum water depth of 5 m. The model boundaries are closed in the north and west with free slip conditions and open in the south and east. Horizontal and vertical discretization schemes, as well as turbulence closure schemes of the model are the same as those used in the model described in Chapter II. Bottom stress is parameterized with a logarithmic formulation, with the

bottom roughness specified as 0.02 m.

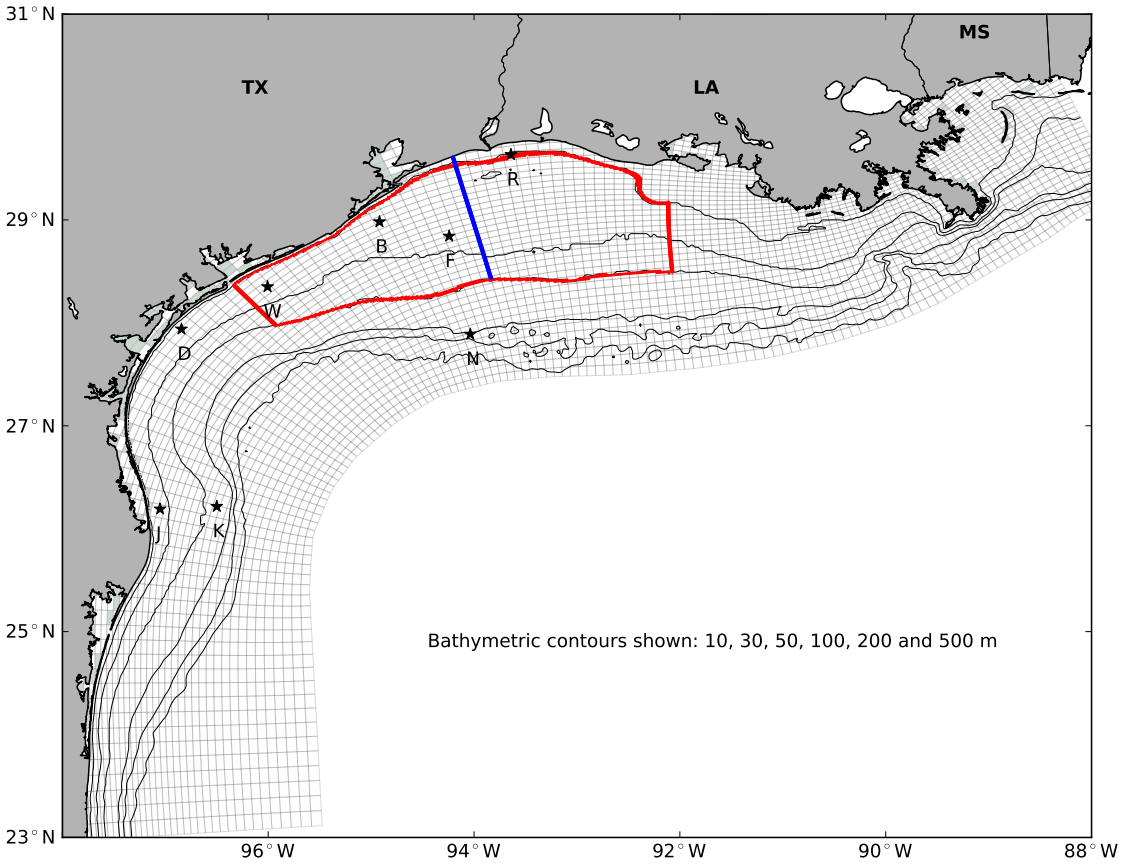

Figure 19. A map of the Texas-Louisiana shelf is shown with the numerical grid of the high-resolution model (3.2) superimposed. The grid is plotted every fifth model point. The bathymetric contours are shown for the 10, 30, 50, 100, 200 and 500 m isobaths. The study region is bounded by the red curves, and the blue line denotes a cross section in the middle of the study region. The black stars mark the locations of the TABS buoy sites.

The model simulation spans the period from 1 February 2003 to 1 January 2012. The initial and open boundary conditions are obtained from the Gulf of Mexico Hybrid Coordinate Ocean Model (GOM-HYCOM) (http:\\www.hycom.org) covering the entire GOM. This nesting gives a reasonable representation of Loop Current eddies in the

model. Atmospheric forcing and fresh water fluxes for the Mississippi and Atchafalaya rivers come from the same datasets as used in the model described in Chapter II, and river discharge from the other seven rivers (the Nueces, San Antonio, Lavaca, Brazos, Trinity, Sabine and Calcasieu Rivers) are obtained from the U.S. Geological Survey Real-Time Water Data for the Nation. This model does not contain tides either. The analyses in this chapter are based on model results of year 2011.

The performance of the model has been extensively evaluated by observational data of surface currents, temperature, 3-dimensional salinity and sea surface elevation in *Zhang et al.* [2012a] and *Zhang et al.* [2012b]. The model has demonstrated positive skills simulating the observed fields of all these variables. Figure 20 shows the comparison between the modeled and the TABS-measured surface along-shore currents. The modeled and observed data are only compared at the inner-shore buoy sites (B, D, F, J, R and W). At each buoy site, the observational data are linearly interpolated onto the model time moments, and then a 33-hr low-band-passing filter is applied to both modeled and observed data to remove near-inertial oscillations. The data are then rotated to the along-shore direction. Since this study involves momentum balance analyses (section 3.3) that are sensitive to the coordinate system in a coastal ocean, it is very important to reasonably define the along-shore and cross-shore axes of the flow. The following methods were tried for the definition of the along-shore direction: (1) major axis of flow based on a principle component analysis (PCA) of multiple-winter currents; (2) major axis of flow based on a PCA of multiple-summer currents; (3) major axis of

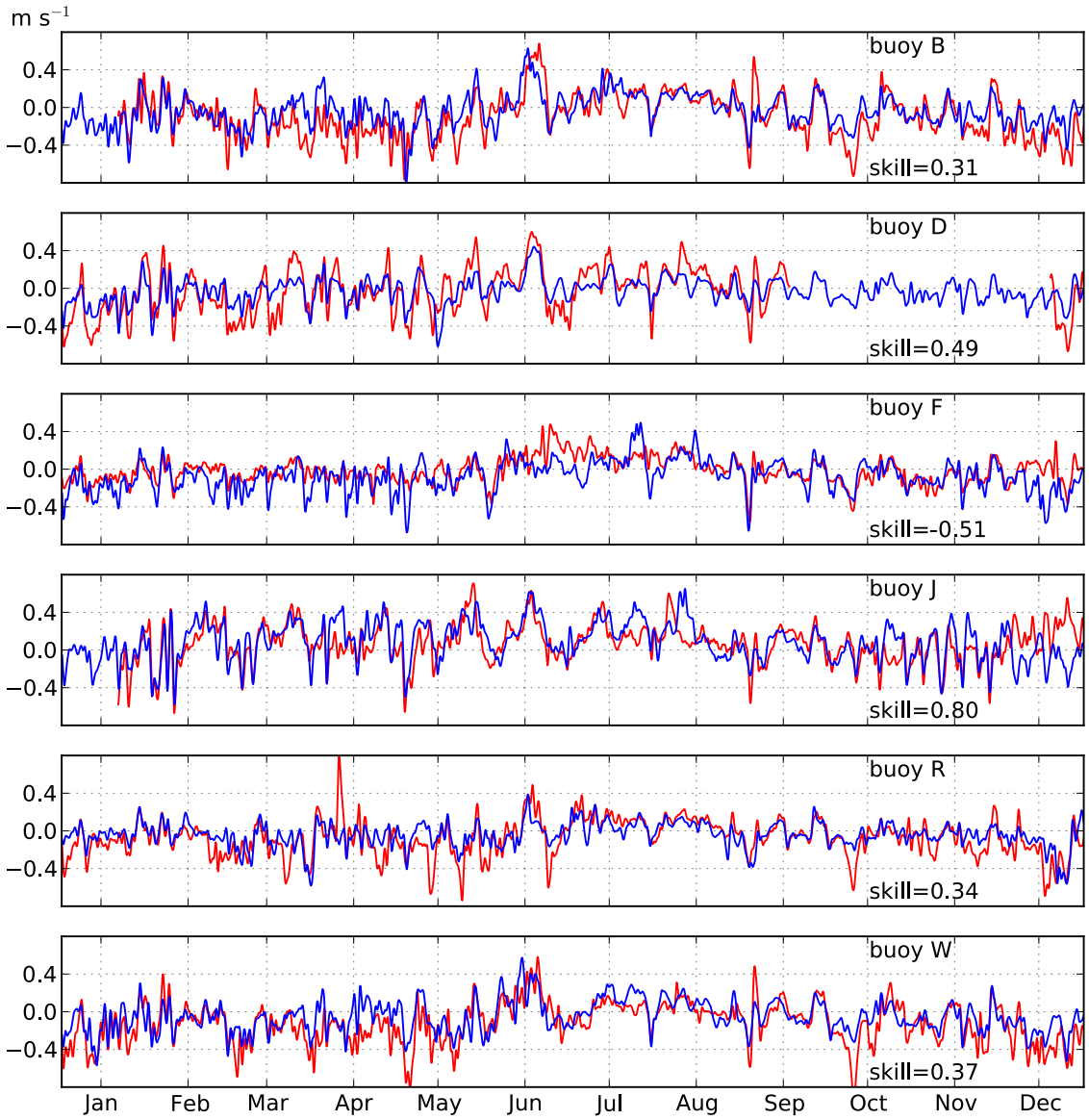

Figure 20. Comparison between the modeled (blue line) and observed (red line) surface along-shore currents after a 33-hr low-band-passing filtering at the inner-shore TABS buoy sites for year 2011.

flow based on a PCA of currents in the entire year of 2011; and (4) direction of minimal gradient of water depth. Method (3) was chosen using the criteria of smallest magnitude of cross-shore flow near the coast and a smooth field of rotation angle.

Figure 20 shows that the variability in the observed surface along-shore current of 2011 is well captured by the model simulation, with positive model skills at most of the inner-shore buoy sites. A detailed comparison between the modeled and observed surface along-shore currents by TABS for February, which will be chosen for momentum balance diagnoses in 3.3, is provided in Table 1 with the major statistical parameters listed. In February, the modeled mean current is in good agreement with the observed mean current at buoy B, D, and W, and the standard deviations of the modeled and

Table 1. Comparisons of statistical parameters for the observed and simulated surface along-shore currents by the model described in 3.2 for February mean at selected TABS buoy sites. The statistical parameters include observational mean, modeled mean, observational standard deviation, modeled standard deviation, model skill and correlation coefficient between the observed and modeled values (r).

February						
Buoy	obs mean ($m\ s^{-1}$)	model mean ($m\ s^{-1}$)	obs std ($m\ s^{-1}$)	model std ($m\ s^{-1}$)	skill	r
B	-0.01	-0.02	0.16	0.16	0.83	0.73
D	-0.03	-0.04	0.23	0.15	0.80	0.79
F	-0.02	-0.06	0.10	0.13	0.47	0.71
J	-0.03	0.02	0.26	0.26	0.77	0.89
R	-0.02	0.01	0.10	0.09	0.82	0.83
W	-0.05	-0.07	0.16	0.14	0.83	0.71

observed data are close at most of the buoys sites. At all of the buoy locations, the model skills and correlations between the modeled and observed currents are positive and high. The good match between the modeled and observed data gives us confidence that the model can capture the dynamics of the wintertime along-shore flow reasonably well.

3.3 Results

3.3.1 Monthly mean structures of plume and along-shore flow

Figure 21 presents profiles of the monthly mean density and along-shore flow during winter and fall seasons along a cross section in the middle of the study region (Figure 19). All of the months shown here are characterized by down-coast wind (except for September, Figure 22), which compresses the plume against the coast and creates fairly vertically-aligned isopycnals. Therefore the front extends from surface to bottom. However, for most months, this bottom-advected plume does not have a sharp density front similar to that shown by *Chapman and Lentz* [1994]. Rather, the isopycnals within the plume are quite evenly spaced in the cross-shore direction, creating a wide density front. This wide front might be viewed as a horizontally stretched version of the narrow front described by *Chapman and Lentz* [1994], and this encourages us to assume a thermal wind balance between the along-shore flow and cross-shore density gradient over the study region with no flow at the bottom. The density structure in September is somewhat different from the other months, as it keeps certain features of the

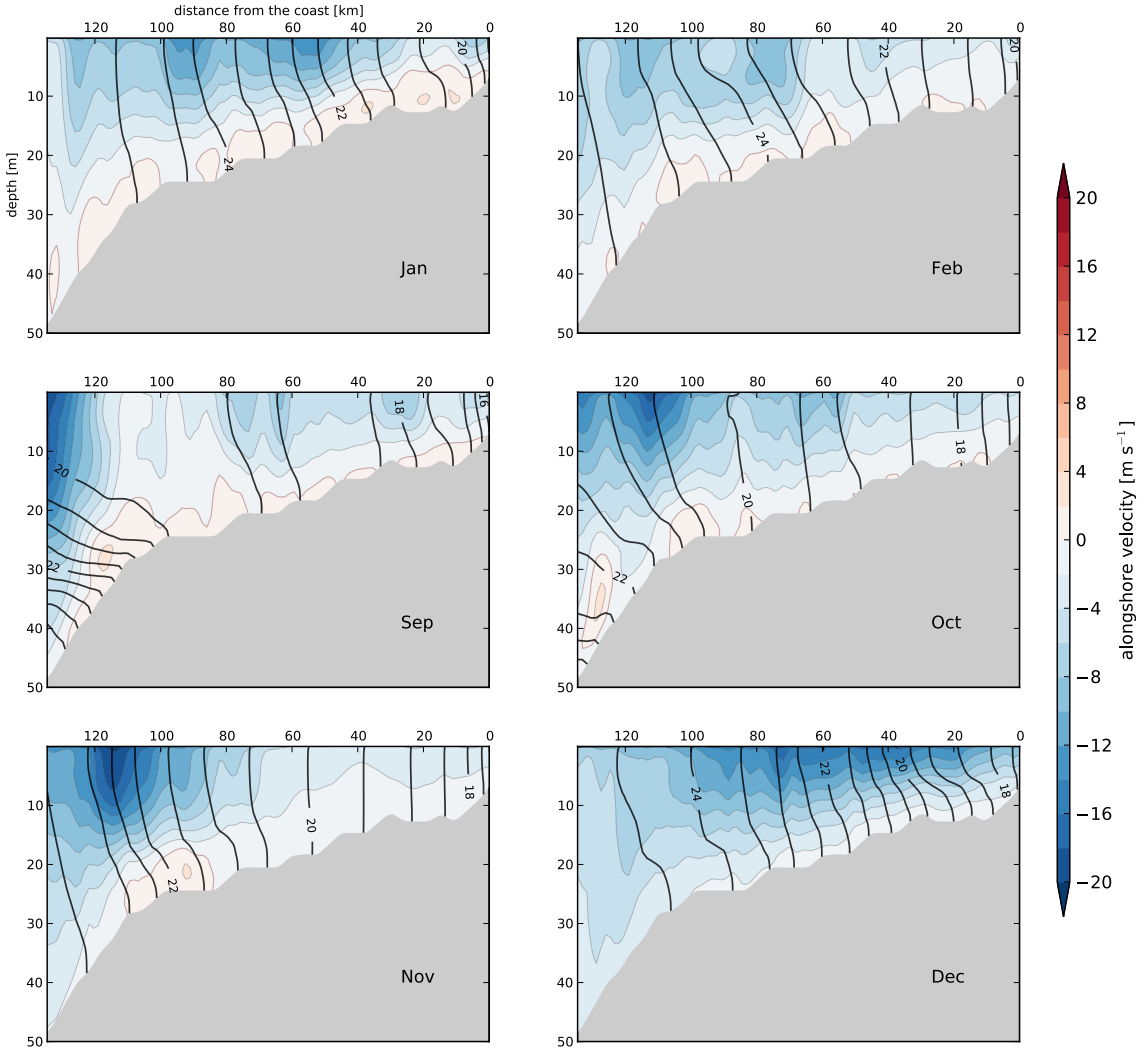

Figure 21. Profiles of monthly mean density (black contour lines) and along-shore flow (colors) during winter and fall months of 2011 on the cross section shown in Figure 19. The density contours are plotted at intervals of 0.5 kg m−3. The thin pink line draws the zero velocity contour line.

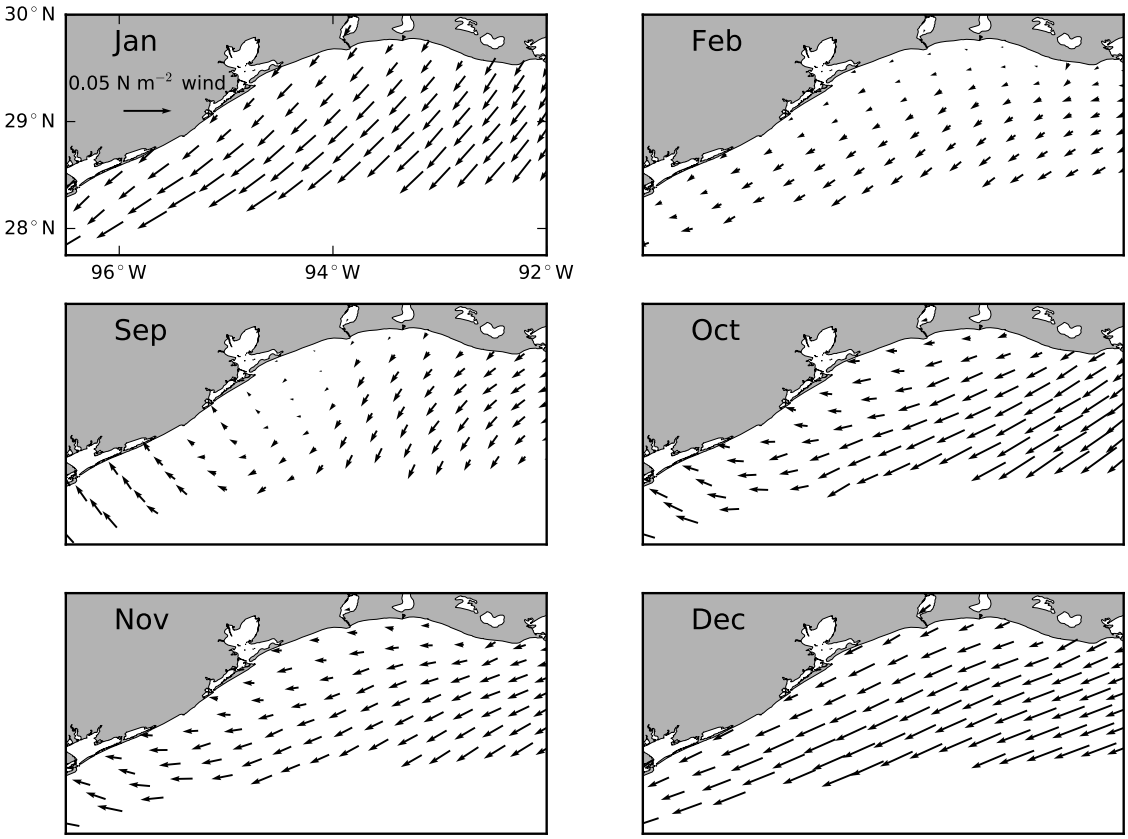

Figure 22. Monthly mean wind stress fields over the Texas-Louisiana shelf inshore of 50-m water depth for winter and fall months of year 2011.

summertime density field, which is beyond the discussion of this study.

As indicated by the thermal wind balance, the cross-shore density gradient, which is positive offshore, creates a substantial vertical shear in the along-shore flow, and the shear acts to reduce the down-coast flow from surface to bottom (Figure 21). The strongest shear appears in January and December corresponding to the largest cross-shore density gradient in these two months, as a result of straining by the strongest down-coast winds (Figure 22). Due to the wide density front, the velocity shear exists

nearly over the entire shelf in all of the months, but is slightly larger in water depths deeper than 20 m (February, October and November). In November, a relatively sharp density front is observed at 100 - 120 km off the coast, generating a strong jet with large vertical shear, and the velocity structure is similar to that of the bottom-advected plume in *Chapman and Lentz* [1994]. A key point in the theory of *Chapman and Lentz* [1994] for the bottom-advected plume is that at the equilibrium state, the vertical shear causes a reversal of the along-shore velocity at the base of the front, and this feature is clearly observed in Figure 21. In January, February, September and October, the buoyancy-induced shear reduces the down-coast flow to zero at a height of two to eight meters above the bottom, and this occurs across most of the shelf. As it goes deeper, the down-coast flow is reversed to up-coast, although the up-coast flow in the bottom boundary layer is generally weak (about 2 cm s^{-1}). In November, the reversal of the along-shore flow only occurs at the base of the sharp density front, which is similar to the case discussed in *Chapman and Lentz* [1994]. In December, although there is a substantial cross-shore density gradient, the alongshore flow is not reversed at bottom (Figure 22). It can be inferred that this is not a steady state situation, so adjustment between buoyancy and along-shore flow will continue. Due to the complex geometry of the Texas-Louisiana shelf, the cross-shore structure of plume varies from one region to another. Density profiles on cross sections west of the Galveston Bay (not shown) reveal that a reversal of the along-shore flow occurs over the entire shelf in November and December as well.

3.3.2 Estimating the thermal-wind-balanced flow

The density and flow patterns of the wintertime bottom-advected plume show consistency with the theory of *Chapman and Lentz* [1994]. This suggests that we can use the thermal wind balance to estimate the along-shore flow, following *Yankovsky and Chapman* [1997]. Here, the critical assumption is that the bottom along-shore velocity is zero across the sea floor. This is reasonable considering that bottom flows are very weak for the case shown in Figure 21. The thermal-wind-balanced flow u_T at position z of the vertical coordinate is given by:

$$u_T(z) = \frac{g}{\rho_0 f}\int_{-H}^{z}\frac{\partial \rho}{\partial y}dz, \tag{7}$$

The symbols in equation 7 are the same as those used in equation 2. The thermal-wind-balanced flow at surface during winter and fall months of 2011 are compared with the modeled surface along-shore flow (which is used to denote the actual flow in this study) in Figure 23. The majority of points fall into the third quadrant, indicating, as expected, that both the thermal-wind-balanced flow and modeled flow are in the down-coast direction. There is overall a good agreement between these two variables, as their relation basically follows the 1-to-1 line, and the average difference between the thermal-wind-balanced flow and actual along-shore flow is close to 0. The slope of the regression line (or best-fit line) is close to 1, and the correlation between the two variables is significant, with the highest correlation coefficient reaching 0.85 in December. These results suggest that the flow derived from the thermal wind balance

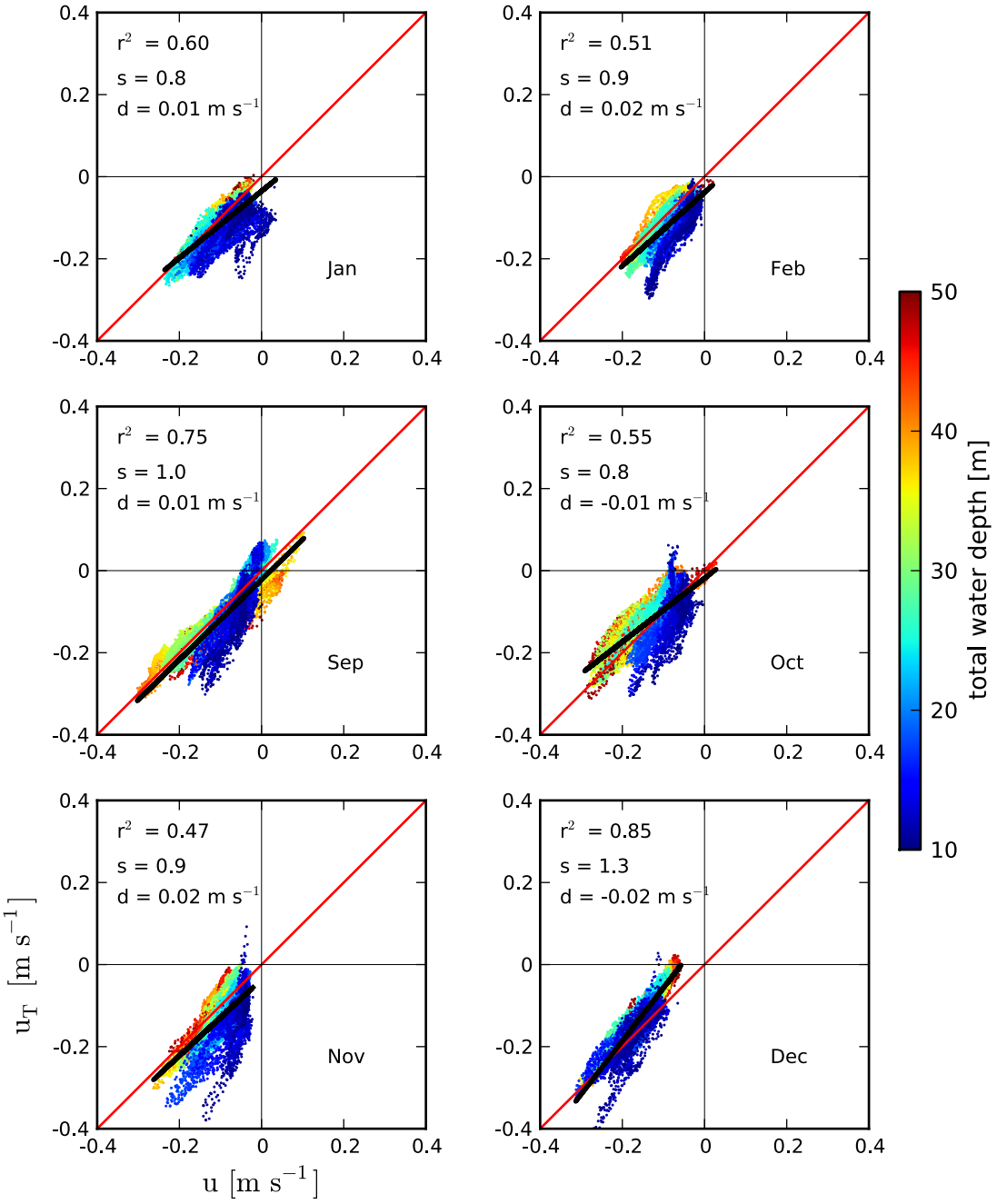

Figure 23. Regression between the monthly mean thermal-wind-balanced flow and modeled along-shore flow at surface for winter and fall months of 2011. The red line is the 1-to-1 line, and the thick, black line is the best-fit line. The regression coefficient (r^2), slope of the best-fit line (s), and averaged difference between the thermal-wind-balanced flow and the modeled along-shore flow (d) are labeled. The difference is defined positive (negative) if the thermal-wind-balanced flow is smaller (larger) than the modeled along-shore flow.

provides a good estimate of the actual along-shore flow. The regression line is slightly below the 1-to-1 line in January, February, September and November, indicating that the thermal-wind-balanced flow is lower than the modeled flow. Such discrepancy is related to the assumption of zero bottom velocity, since in these cases there is weak up-coast flow at bottom. The discrepancy tends to occur in water depths shallower than 20 m, particularly near 10 m. In water deeper than 20 m, the thermal-wind-balanced flow is basically in line with the modeled flow. This is because the along-shore wind is generally weak near the coast, resulting in weak along-shore currents, and although the horizontal density gradient is not very strong in this region, it is capable of reversing the currents to relatively large up-coast values at bottom (see Figure 21a). Therefore the assumption of zero bottom flow may not be very appropriate for this region. Also, this is the region that first feels the cross-shore advection of fresh water and may be dynamically more unstable than deeper water. On the whole, in winter and fall seasons the thermal wind relation plays a dominant role in the along-shore flow dynamics, and the flow derived from this relation explains the majority of the total along-shore flow.

3.3.3 Momentum balance analyses

In this section, momentum balances are analyzed to diagnose the wintertime flow dynamics. In particular, such analyses aim to explain the dominance of the thermal wind balance in the along-shore flow dynamics and the mechanisms controlling the bottom flow. Momentum balance analyses have been widely employed in shelf circulation

studies [*Fewings and Lentz*, 2010; *Lentz et al.*, 1999; *Liu and Weisberg*, 2005; *Tilburg and Garvine*, 2003], but most are focused on the depth-averaged flow. A 3-dimensional momentum analysis is required for diagnosing flows with substantial vertical structure, as in this study case. An examination of the momentum budgets revealed that the local acceleration, nonlinear and horizontal viscosity terms are generally small compared to other terms. Thus, the 3-dimensional along-shore and cross-shore momentum equations can be reduced to

$$-\frac{1}{\rho_0}\frac{\partial p}{\partial x} + fv + \frac{\partial}{\partial z}(K_V \frac{\partial u}{\partial z}) = 0\,, \tag{8}$$

and

$$-\frac{1}{\rho_0}\frac{\partial p}{\partial y} - fu + \frac{\partial}{\partial z}(K_V \frac{\partial v}{\partial z}) = 0\,, \tag{9}$$

respectively, where (u, v) are the along-shore and cross-shore components of velocity, $(\partial p/\partial x, \partial p/\partial y)$ are the along-shore and cross-shore pressure gradients, and K_V is the vertical eddy viscosity coefficient. A winter month, February, is chosen for the momentum balance diagnose. The analysis is first focused on the planeview of momentum balance at the bottom and surface of ocean in the study region. Since results depend strongly on the definition of along-shore, and it is difficult to find a consistent definition for the whole region, the momentum terms are plotted as vectors. This way the along-shore and cross-shore momentum balances can be shown at the same time. At each point of the region, the pressure gradient vector is plotted first. It is followed by the plotting of the Coriolis acceleration and then the vertical eddy viscosity vectors. The pressure gradient vector originates from the geographic location of the point, while the

vectors of the Coriolis and viscosity terms start from the ending point of the vector preceding them in plotting. This way of plotting is illustrated in Figure 24. If the three vectors form a closed triangle, it means that the momentum budget can be completely described by the three terms. The shape of the triangle indicates the character of momentum balance, and three types of momentum balance composed by the pressure gradient, Coriolis and vertical eddy viscosity terms are shown in Figure 24.

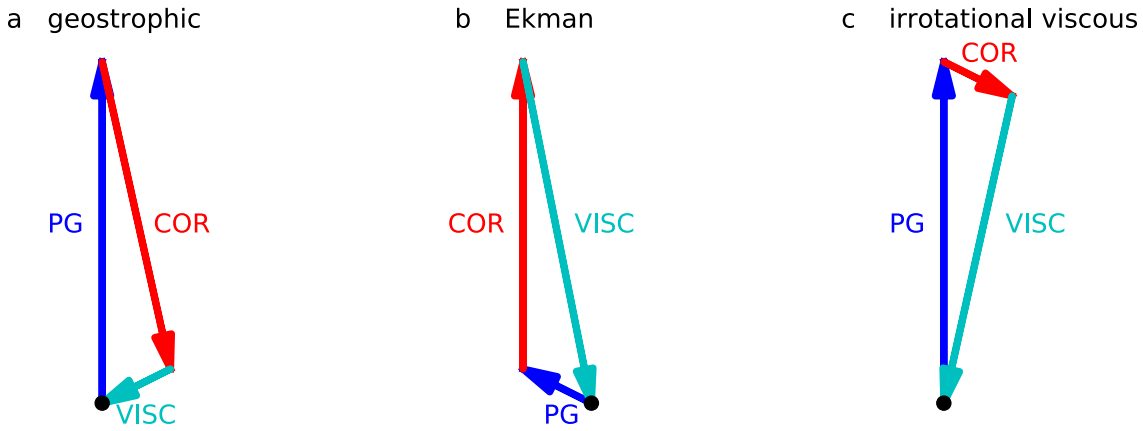

Figure 24. Illustration of vector plot of the momentum balance composed by the pressure gradient (PG), Coriolis acceleration (COR) and vertical eddy viscosity (VISC) terms. The black dot is the starting point for the PG vector that is first plotted. The COR and VISC vectors are plotted thereafter and they start from the ending point of the vector preceding them in plotting. Three types of momentum balance are shown. For type a, the dominant balance is between PG and COR, corresponding to a geostrophic flow (see Figure 25b). For type b, the dominant balance is between COR and VISC, corresponding to an Ekman flow. For type c, the dominant balance is between PG and VISC, corresponding to an irrotational viscous flow (see Figure 25a).

Figure 25a shows the bottom momentum balance for February mean in the study region. We can see that at most of the points, the momentum budget is almost closed by the pressure gradient, Coriolis and eddy viscosity terms (this actually justifies the insignificance of the neglected terms in equation 8 and 9). There is in general a tendency for the momentum terms to decrease offshore; and by the 50-m isobath their magnitudes have been substantially reduced. The character of the momentum balance is similar at different points of the study area. Therefore, a detailed analysis is performed for a point on the cross section in 20 m of water. In the cross-shore momentum budget, the dominant balance is between the pressure gradient term and the eddy viscosity term, with the former slightly larger than the later and the small difference explained by the Coriolis term. The major balance in the along-shore momentum budget is between the eddy viscosity term and the Coriolis term, i.e., an Ekman balance. In *MacCready and Rhines* [1993], at the equilibrium state of the bottom boundary layer, the cross-shore pressure gradient of the initial flow is canceled out by the buoyancy force at bottom, and there is no need for a viscous boundary layer to exist. However, in the case shown in Figure 25a, the eddy viscosity term at bottom is not zero due to the existence of a small cross-shore flow, and the cross-shore pressure gradient is adjusted by the buoyancy force to the extent that it can almost balance the eddy viscosity, leaving a small Coriolis term. On the other hand, the cross-shore flow, which is onshore, is generated by the along-shore stress associated with the weak up-coast bottom flow through the Ekman balance. These processes agree with the theory of *Chapman and Lentz* [1994] on the dynamics at the base of the front (see their Figure 4).

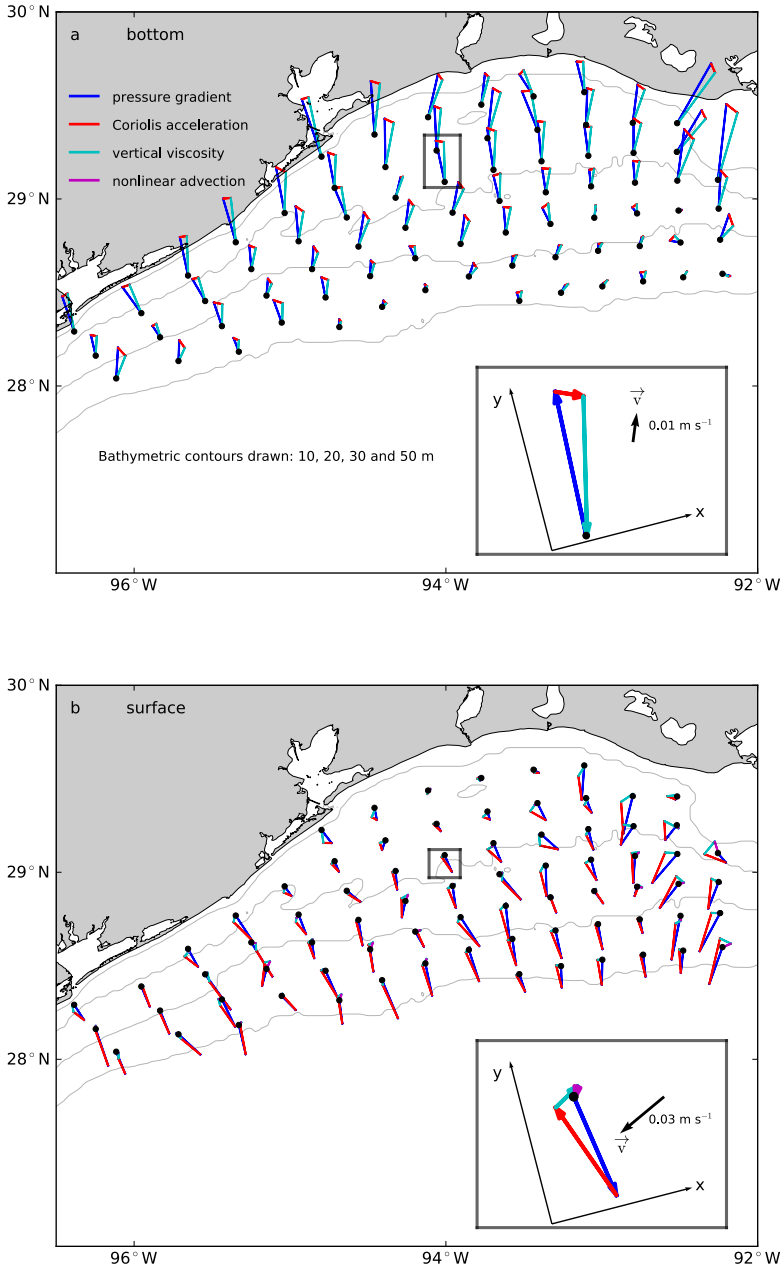

Figure 25. A geographic map showing the (a) bottom and (b) surface momentum balances of February mean at selected points of the study region. The blue, red, cyan and purple arrows plot the vectors of the pressure gradient ($-1/\rho_0(\partial p/\partial x)$, $-1/\rho_0(\partial p/\partial x)$), Coriolis acceleration (fv, $-fu$), vertical eddy viscosity ($\partial/\partial z(\partial u/\partial z), \partial/\partial z(\partial v/\partial z)$) and nonlinear terms, respectively. An enlargement of the momentum terms for a point in 20-m water of the cross section is given in the lower right corner, with directions of the vectors more clearly shown and the along-shore (x) and cross-shore (y) axes drawn. The velocity vector ($\vec{v}$) at this point is also plotted, with its magnitude labeled. Note that scales for the bottom and surface vectors are different in consideration of visual effects.

Figure 25b shows the February mean momentum budget at the surface. The character of the momentum balance is still quite consistent over the study region, and the momentum budget is dominated by the pressure gradient and Coriolis acceleration, with a small vertical eddy viscosity term making up the difference at most points. Therefore the flow is in geostrophic balance. At a few locations the nonlinear term also plays a role, and thus is plotted as well. The dominance of the geostrophic balance in the cross-shore momentum budget for mid-depth water has been widely found in studies of continental shelf circulation [*Fewings and Lentz*, 2010; *Lentz et al.*, 1999; *Liu and Weisberg*, 2005] and studies of coastal plumes [*Garvine*, 1995; *Munchow and Garvine*, 1993]. Inshore of 20 m, the eddy viscosity term plays a larger role, but in general all the momentum terms are small in this region.

Figure 26 displays profiles of the major cross-shore momentum terms of February mean on the cross section. Away from the bottom boundary and coast, the pressure gradient (a) and Coriolis (b) terms show similar patterns, and their difference (c) is mainly explained by the vertical eddy viscosity term (d), indicating that in wintertime, the three-way balance in the cross-shore momentum equation is fairly robust throughout the water column. Except in the middle of the ocean where the viscosity term is relatively large, the geostrophic balance is dominant in most of the interior and surface ocean. For a geostrophic balance, under the hydrostatic assumption, the shear of along-shore flow is in thermal wind balance with the cross-shore density gradient. This explains why in

winter and fall months the thermal-wind-balanced flow is a good approximation of the actual along-shore flow.

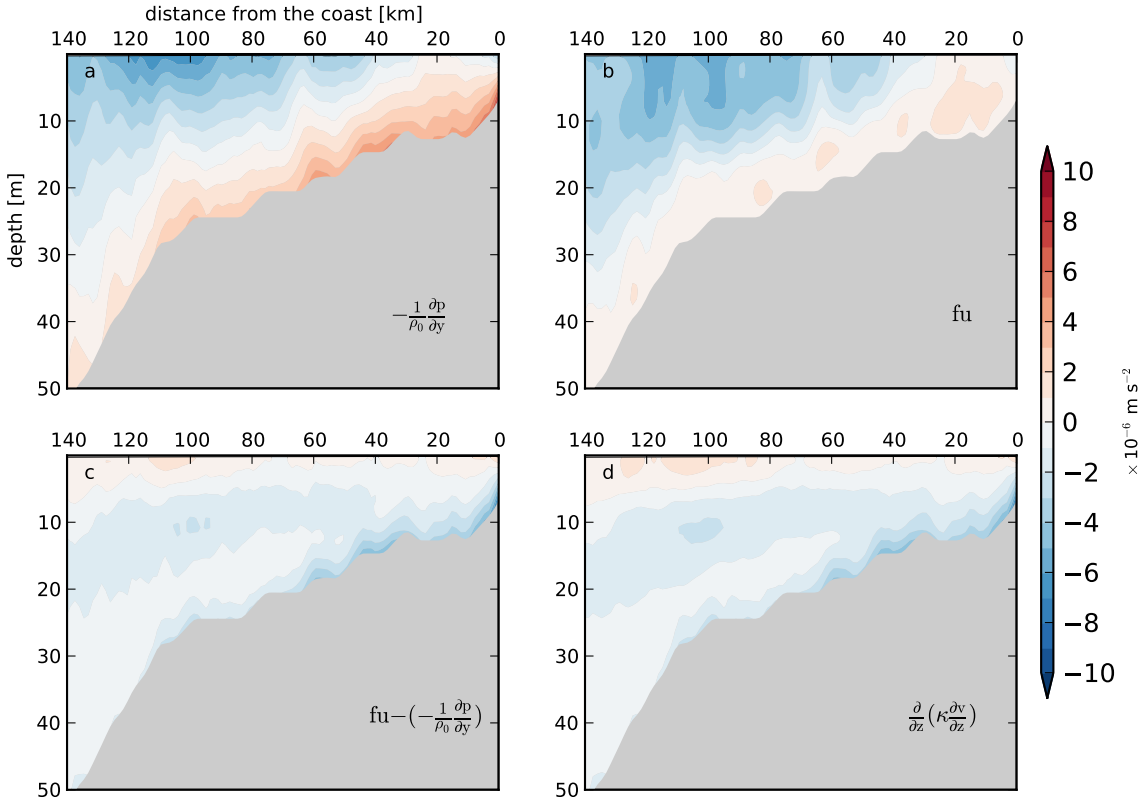

Figure 26. Cross-sectional profiles of the major terms: (a) pressure gradient, (b) Coriolis acceleration and (d) vertical eddy viscosity in the February mean cross-shore momentum budget and (c) the difference between the Coriolis and pressure gradient terms. Note that the Coriolis term is plotted as fu (instead of $-fu$ as in equation 9) to be more clearly compared with the pressure gradient term.

3.4 Discussion

As mentioned above, the Mississippi-Atchafalaya river plume is strained by the along-shore wind, and the bottom-advected plume pattern in wintertime is maintained by

down-coast wind. An interesting question to know is that how long it takes the river plume to adjust to a change in the along-shore wind forcing. The variable synoptic-scale wind over the Texas- Louisiana shelf in wintertime [*Wang et al.*, 1998; *Zhang and Hetland*, 2012] provides an opportunity to examine the response of the Mississippi-Atchafalaya river plume under alternating down-coast and up-coast winds. Figure 27 shows the plume behavior on the cross section during a wintertime period when the along-shore component of wind has reversals. On 27 January, at the onset of an up-coast wind event, the isohalines are aligned fairly vertically except at the bottom, and the offshore edge of the plume (indicated by the salinity value of 33 psu, following *Hetland et al.* [2012]) at surface is about 75 km off the coast (a). The up-coast wind strengthens from 27 January to the midday of 28 January (Figure 27, bottom), and persists until late afternoon of 29 January. During this time, the plume edge has extended from 75 km to 105 km off the coast (early morning of 30 January, Figure 27d), and the isohalines have shown a substantial tilting. The along-shore wind changes direction on 29 January, and the down-coast wind persists until the afternoon of 1 February. During early morning of 30 January through the midday of 31 January, the weak down-coast wind does not induce a large change in the density field, and the plume edge basically stays at the 105-km location. From the midday of 31 January to late afternoon of 1 February, the relatively strong down-coast wind leads to a slight reduction in the isohaline tilting and retreat of the plume edge on 2 February (f). A pulse of up-coast wind occurring on 1 February and 2 February does not seem to have a large impact on the density field, and the pattern of isohalines during 2 February through 5 February are mainly subject to the

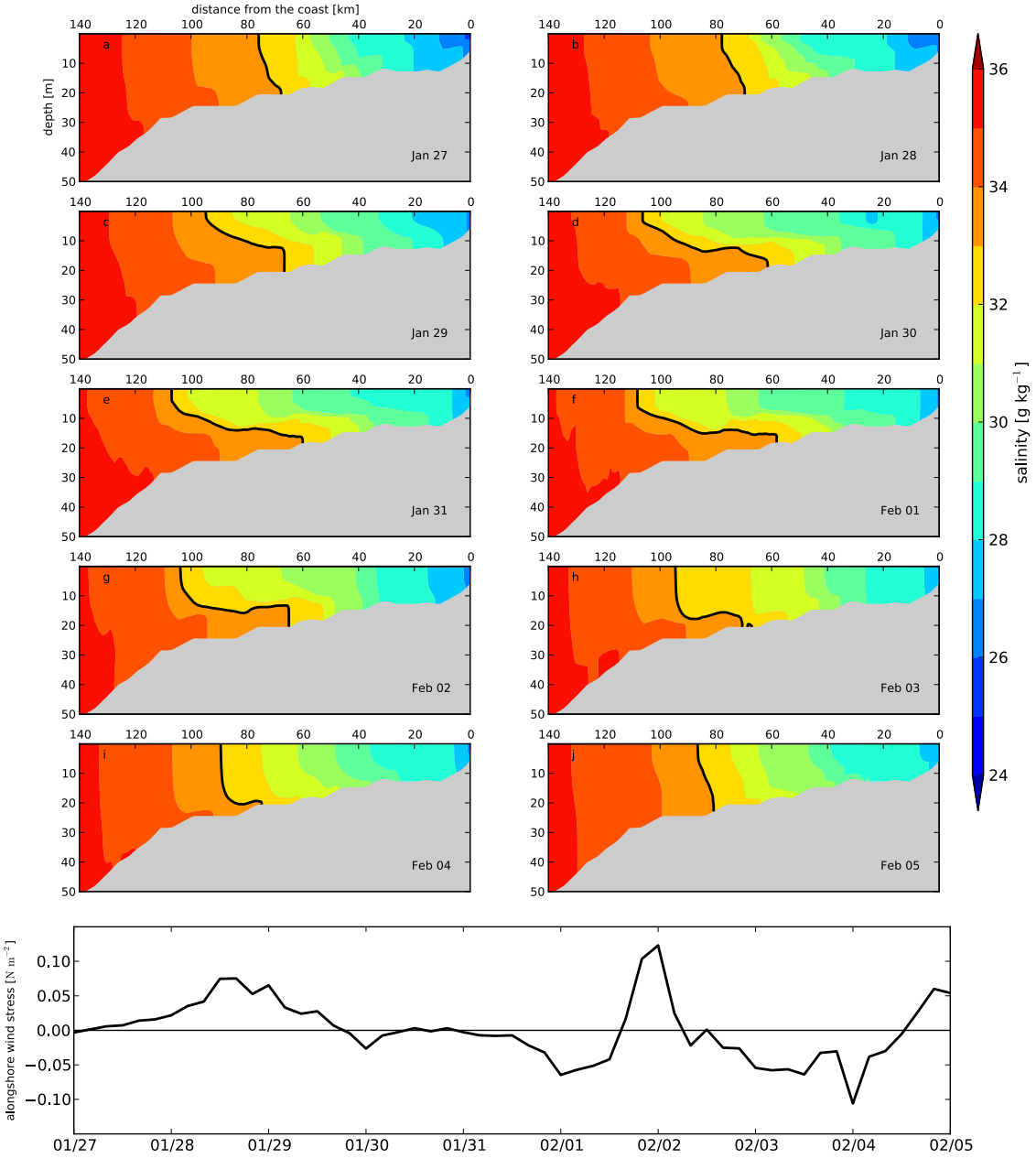

Figure 27. A time sequence of the cross-sectional profile of salinity (a-g) showing the adjustment of the plume to alternating up-coast and down-coast wind forcing and the time series of the cross-section-averaged along-shore wind stress in the same time period. The initial time is 00:00 of 27 January, and the time interval between consecutive plots is 24 hours. The thick, black line labels the 33 psu isohaline, which is an indication of the offshore edge of the plume.

effect of down-coast wind and shows a substantial steepening; on 5 February, the plume has returned to a bottom-advected pattern. These analyses suggest that the density field has a fast response to the wind forcing, and the plume pattern can be changed by wind within a few days. *Whitney and Garvine* [2005] estimated the wind strain timescale for a plume width by considering the time it takes the plume width to be changed by 50%, which is

$$t = \frac{Lh\rho f}{16\tau^{sx}} \tag{10}$$

where L is the plume width, h is the trapping depth of the plume and τ^{sx} is the along-shore wind stress. For the Mississippi-Atchafalaya river plume, if we take the plume width as 50 km, the trapping depth as 20 m (inferred from Figure 27, where intensified horizontal density gradient lies) and an average down-coast/up-coast wind stress of 0.03 N m^{-2}, equation 10 will give a timescale of ~36 hrs. Considering the plume behavior on the cross section during 28 January through 30 January, the plume width at surface has changed by 30 km, which is slightly larger than half the plume width (25 km), so the timescale of this change (2 days) is basically consistent with the estimated time.

It needs to be addressed that this study does not isolate the buoyancy forcing effect on the along-shore flow, which could be done by creating a no-wind environment. Rather, it investigates the buoyancy forcing in the context of realistic along-shore wind forcing. It is demonstrated that the buoyancy-driven along-shore current can explain the majority of the actual along-shore current in non-summer. This does not contradict the conclusions

drawn from previous studies, which argued that along-shore wind is a major forcing mechanism for the along-shore flow, since there is a significant correlation between the along-shore flow and along-shore wind on seasonal scale [Cho et al., 1998; Cochrane and Kelly, 1986; Jarosz and Murray, 2005] as well as in the weather band (2.3.3). In the coexistence of wind and a buoyant plume, the high correlation between the along-shore wind and along-shore flow can be understood by their relations with the plume pattern (or the density field), which can quickly adjust to changing along-shore wind, as shown in the analysis above, and then modulate the flow field.

CHAPTER IV

CONCLUSIONS

In this dissertation, numerical investigations are conducted for the along-shore circulation over the Texas-Louisiana continental shelf inshore of 50-m water depth under the influences of wind and buoyancy forcing. Two relevant scientific problems are studied. The first problem is a specific feature of the along-shore flow field, namely convergent coastal flows, which are characterized by the encountering of up-coast flows over the southern shelf and down-coast flows over the northern shelf. The second problem is about the dynamics of seasonal-scale buoyancy-driven circulation in the context of realistic wind forcing. The conclusions of these two studies are provided separately below.

4.1 Convergent along-shore flows

Convergent surface along-shore flows on the inner Texas-Louisiana shelf were investigated with a medium-resolution numerical model covering the entire Gulf of Mexico based on the Regional Ocean Modeling System (ROMS). Comparisons with observations show that the model has a reasonable ability to reproduce observed shelf-scale surface currents, sea-surface height and 3-dimensional salinity fields.

Convergent flows are studied on both the weather band and seasonal timescales. The model predicted convergence locations are supported by moored current observations. This study finds a close relation between the formation of convergent flows and spatial variation in the along-shore component of wind forcing. Convergent flows are associated with broad-scale landward-blowing winds. While the wind direction is nearly uniform over the entire shelf, the along-shore component of wind changes with the curving coastline. The curving coastline causes the along-shore wind to undergo a reversal from the south Texas coast to the Louisiana coast. The reversal in the along-shore wind direction is mirrored in the along-shore current direction, resulting in a convergence zone. For the weather band, convergence events can last from several hours to several days, and in winter seasons they are usually ended by the passage of cold fronts that drive intensified down-coast currents along the entire shelf.

In wintertime, surface along-shore currents respond swiftly to along-shore wind variations for most of the inner shelf region, and the two variables follow a relatively linear relationship with high correlation, confirming that the along-shore wind is the dominant factor in the formation of convergent along-shore flows. In summertime, both winds and currents are weak and currents are less sensitive to wind changes, and under the more disorganized flow patterns convergent events are hard to distinguish. This is attributed in part to the longer response time of the currents to the wind.

The convergence points for currents and wind are not co-located. Usually, convergent currents rather occur down-coast of convergent winds. Two factors contribute to the down-coast shift of the convergent currents: buoyancy forcing that can drive down-coast currents through the offshore density gradient associated with the Mississippi-Atchafalaya river plume, and continental shelf waves that propagate down-coast and generate non-locally-forced currents. Results from a sensitivity model run that excludes river discharge suggest that buoyancy forcing is most likely the primary factor for causing the offset between the convergent currents and winds, since such offset almost disappears when buoyancy forcing from the rivers is turned off. Continental shelf waves seem to play a negligible role. Also, the magnitude of buoyancy-driven along-shore currents estimated from the thermal wind balance indicates that the buoyancy-driven flow is similar in magnitude to the observed down-coast flow under no wind forcing.

As the weather-band winds have a large temporal variability, the location of convergent along-shore wind varies substantially with time, and can occur over a broad stretch of the Texas and Louisiana coastlines. The weather-band convergent currents also show a temporal variability, but their occurrence is basically confined between Galveston Bay and Baffin Bay of Texas. No specific temporal pattern is found for the weather-band convergence. However, the monthly mean convergent winds and currents clearly reveal a seasonal pattern based on both model and observational results. Convergence typically appears in the southern section of the Texas-Louisiana shelf in early spring and marches up-coast with the transition of prevailing winds over the shelf from down-coast in winter

to up-coast in summer. This up-coast migration stops in mid-summer and, as down-coast winds begin to dominate again, the convergence location retreats southward until late winter. The seasonal migration of convergence is consistent with findings from previous studies of the Texas-Louisiana shelf circulation [*Morey et al.*, 2005; *Zavala-Hidalgo et al.*, 2003]. In this study, it is demonstrated that such seasonal migration pattern has interannual variability. In a year with stronger summertime up-coast wind, the convergence location intrudes further up-coast in the summer seasons.

4.2 Buoyancy-driven seasonal along-shore circulation in the non-summer flow regime

A high-resolution numerical model covering the entire Texas-Louisiana shelf and slope region is employed to investigate the dynamics of the seasonal buoyancy-driven circulation over the Texas-Louisiana shelf in the non-summer flow regime. The buoyancy forcing drives along-shore flow through a thermal wind balance. In non-summer, under down-coast wind forcing, the Mississippi-Atchafalaya river plume has a bottom-advected pattern, for which the plume front extends from surface to bottom of the ocean. It is the first time that dynamics of the bottom-advected Mississippi-Atchafalaya river plume has been studied. Results showed that, unlike a typically described bottom-advected plume that is created in a no-wind environment, the Mississippi-Atchafalaya river plume has a fairly wide density front that spans nearly across the entire shelf. Under the wide front, the vertical shear in the along-shore flow

resulting from the cross-shore density gradient reverses the along-shore velocity from down-coast at surface to slightly up-coast at the bottom across most of the shelf. The surface flow derived from the thermal wind balance with an assumption of zero bottom velocity agrees well with the actual surface along-shore flow, indicating that the thermal wind balance plays a dominant role in the along-shore flow dynamics in winter and fall, and zero bottom velocity is a valid assumption. The dominant role of the thermal wind balance in the alongshore flow dynamics is supported by momentum balance analyses, which reveal that in a large portion of the surface and interior ocean, the cross-shore momentum budget is dominated by the geostrophic balance, and therefore, under a hydrostatic assumption, the vertical shear of alongshore flow is in thermal wind balance with the cross-shore density gradient in the plume. A practical aspect of this study is that, based on the diagnostic results shown above, in wintertime, the alongshore flow on the Texas-Louisiana shelf can be roughly estimated by the density structure, and no other information needs to be provided.

REFERENCES

Bianchi, T., S. DiMarco, J. Cowan, R. Hetland, P. Chapman, J. Day, and M. Allison (2010), The science of hypoxia in the Northern Gulf of Mexico: a review, *Sci. Total. Environ.*, *408*(7), 1471-1484.

Bogden, P. S., P. Malanotte-Rizzoli, and R. Signell (1996), Open-ocean boundary conditions from interior data: Local and remote forcing of Massachusetts Bay, *J. Geophys. Res*, *101*, 6487-6500.

Chapman, D. C. (1985), Numerical treatment of cross-shelf open boundaries in a barotropic coastal ocean model, *J. Phys. Oceanogr.*, *15*(8), 1060-1075.

Chapman, D. C., and S. J. Lentz (1994), Trapping of a coastal density front by the bottom boundary layer, *J. Phys. Oceanogr.*, *24*(7), 1464-1479.

Cho, K., R. O. Reid, and W. D. Nowlin (1998), Objectively mapped stream function fields on the Texas-Louisiana shelf based on 32 months of moored current meter data, *J. Geophys. Res*, *103*, 10377-10390.

Clarke, A. J., and K. Brink (1985), The response of stratified, frictional flow of shelf and slope waters to fluctuating large-scale, low-frequency wind forcing, *J. Phys. Oceanogr.*, *15*(4), 439-453.

Cochrane, J., and F. Kelly (1986), Low-frequency circulation on the Texas-Louisiana continental shelf, *J. Geophys. Res*, *91*(C9), 10645-10659.

Csanady, G. (1978), The arrested topographic wave, *J. Phys. Oceanogr.*, *8*, 47-62.

DiMarco, S. F., P. Chapman, N. Walker, and R. D. Hetland (2010), Does local topography control hypoxia on the eastern Texas–Louisiana shelf?, *J. Mar. Syst.*, *80*(1), 25-35.

DiMarco, S. F., and R. O. Reid (1998), Characterization of the principal tidal current constituents on the Texas-Louisiana shelf, *J. Geophys. Res*, *103*(C2), 3093-3109.

Feng, Y., S. DiMarco, and G. Jackson (2012), Relative role of wind forcing and riverine nutrient input on the extent of hypoxia in the northern Gulf of Mexico, *Geophys. Res. Lett.*, *39*(9), L09601.

Fewings, M. R., and S. J. Lentz (2010), Momentum balances on the inner continental shelf at Martha's Vineyard Coastal Observatory, *J. Geophys. Res*, *115*(C12), C12023.

Flather, R. (1976), A tidal model of the northwest European continental shelf, *Mem. Soc. R. Sci. Liege*, *10*(6), 141-164.

Fong, D. A., W. R. Geyer, and R. P. Signell (1997), The wind-forced response on a buoyant coastal current: Observations of the western Gulf of Maine plume, *J. Mar. Syst.*, *12*(1), 69-81.

Garvine, R. W. (1995), A dynamical system for classifying buoyant coastal discharges, *Cont. Shelf. Res.*, *15*(13), 1585-1596.

Gill, A., and E. Schumann (1974), The generation of long shelf waves by the wind, *J. Phys. Oceanogr.*, *4*, 83-90.

Haidvogel, D. B., H. G. Arango, K. Hedstrom, A. Beckmann, P. Malanotte-Rizzoli, and A. F. Shchepetkin (2000), Model evaluation experiments in the North Atlantic Basin: simulations in nonlinear terrain-following coordinates, *Dynam. Atmos. Oceans*, *32*(3), 239-281.

Hetland, R. D. (2006), Event-driven model skill assessment, *Ocean Modell.*, *11*(1), 214-223.

Hetland, R. D., and L. Campbell (2007), Convergent blooms of Karenia brevis along the Texas coast, *Geophys. Res. Lett.*, *34*(19), L19604.

Hetland, R. D., and S. F. DiMarco (2011), Skill assessment of a hydrodynamic model of circulation over the Texas–Louisiana continental shelf, *Ocean Modell.*, *43-44*, 64-76.

Hetland, R. D., K. Fennel, C. K. Harris, J. Kaihatu, K. Xu, and S. F. DiMarco (2012), Integrated bio-physical modeling of Louisiana-Texas (LATEX) Shelf, U.S. Department of the Interior, Bureau of Ocean Energy Management Gulf of Mexico Region, New Orleans, LA.

Hunter, R. E., L. E. Garrison, and G. W. Hill (1974), Maps showing the drift patterns along the south Texas coast, *U.S. Geol. Surv. Misc. Field Stud. Map*, *MF-623*.

Jarosz, E., and S. P. Murray (2005), Velocity and transport characteristics of the Louisiana-Texas coastal current, in *Circulation in the Gulf of Mexico: Observations and Models, Geophys. Monogr. Ser.*,vol. 161, edited by W. Sturges and A. Lugo-Fernandez, pp. 143-156, AGU, Washington, D. C.

Leipper (1954), Physical oceanography of the Gulf of Mexico: Gulf of Mexico, its origins, waters and marine life, *Fish. Bull.*, *55*, 119-137.

Lentz, S., R. Guza, S. Elgar, F. Feddersen, and T. Herbers (1999), Momentum balances on the North Carolina inner shelf, *J. Geophys. Res*, *104*(C8), 18205-18226.

Lentz, S. J. (2008), Observations and a model of the mean circulation over the Middle Atlantic Bight continental shelf, *J. Phys. Oceanogr.*, *38*(6), 1203-1221.

Lentz, S. J., and M. R. Fewings (2012), The wind-and wave-driven inner-shelf circulation, *Annual Review of Marine Science*, *4*, 317-343.

Li, Y., W. D. Nowlin Jr, and R. O. Reid (1996), Spatial-scale analysis of hydrographic data over the Texas-Louisiana continental shelf, *J. Geophys. Res*, *101*(C9), 20595-20605.

Liu, Y., and R. H. Weisberg (2005), Momentum balance diagnoses for the West Florida Shelf, *Cont. Shelf. Res.*, *25*(17), 2054-2074.

MacCready, P., and P. B. Rhines (1993), Slippery bottom boundary layers on a slope, *J. Phys. Oceanogr.*, *23*(1), 5-22.

Marta‐Almeida, M., R. D. Hetland, and X. Zhang (2013), Evaluation of model nesting performance on the Texas‐Louisiana continental shelf, *J. Geophys. Res*, *118*, 1-16.

Mellor, G. L., and T. Yamada (1982), Development of a turbulence closure model for geophysical fluid problems, *Rev. Geophys.*, *20*(4), 851-875.

Morey, S. L., J. Zavala-Hidalgo, and J. J. O'Brien (2005), The seasonal variability of continental shelf circulation in the northern and western Gulf of Mexico from a high-resolution numerical model, in *Circulation in the Gulf of Mexico: Observations and Models, Geophys. Monogr. Ser.*,vol. 161, edited by W. Sturges and A. Lugo-Fernandez, pp. 203-218, AGU, Washington, D. C.

Munchow, A., and R. W. Garvine (1993), Buoyancy and wind forcing of a coastal current, *J. Mar. Res.*, *51*(2), 293-322.

Nowlin, W. D. (1998), *Texas-Louisiana shelf circulation and transport processes study: Synthesis report*, US Department of the Interior, Minerals Management Service, Gulf of Mexico OCS Region.

Nowlin, W. D., A. E. Jochens, S. F. DiMarco, R. O. Reid, and M. K. Howard (2005), Low-frequency circulation over the Texas-Louisiana continental shelf, in *Circulation in the Gulf of Mexico: Observations and Models, Geophys. Monogr. Ser.*,vol. 161, edited by W. Sturges and A. Lugo-Fernandez, pp. 219-240, AGU, Washington, D. C.

Nowlin, W. D., A. E. Jochens, R. O. Reid, and S. F. Dimarco (1998), Texas-Louisiana shelf circulation and transport process study: synthesis report, vol. I, Technical report, , *Tech. Rep. OCS Study MMS 98-0035*, Miner. Manage. Serv., U.S. Dep. of the Inter., New Orleans, La.

Oey, L. Y. (1995), Eddy-and wind-forced shelf circulation, *J. Geophys. Res*, *100*, 8621-8621.

Sanders, T. M., and R. W. Garvine (2001), Fresh water delivery to the continental shelf and subsequent mixing: An observational study, *J. Geophys. Res*, *106*(C11), 27087-27101.

Shchepetkin, A. F., and J. C. McWilliams (2005), The regional oceanic modeling system (ROMS): a split-explicit, free-surface, topography-following-coordinate oceanic model, *Ocean Modell.*, *9*(4), 347-404.

Tilburg, C. E., and R. W. Garvine (2003), Three-dimensional flow in a shallow coastal upwelling zone: Alongshore convergence and divergence on the New Jersey shelf, *J. Phys. Oceanogr.*, *33*(10), 2113-2125.

Wang, W., W. D. Nowlin, and R. O. Reid (1998), Analyzed surface meteorological fields over the northwestern Gulf of Mexico for 1992-94: Mean, seasonal, and monthly patterns, *Mon. Weather. Rev.*, *126*(11), 2864-2883.

Watson, R. L., and E. W. Behrens (1970), Nearshore surface currents, southeastern Texas Gulf coast, *Contrib. Mar. Sci.*, *15*, 133-143.

Whitney, M. M., and R. W. Garvine (2005), Wind influence on a coastal buoyant outflow, *J. Geophys. Res*, *110*(C3), C03014.

Wiseman, W. J., N. Rabalais, R. Turner, S. Dinnel, and A. MacNaughton (1997), Seasonal and interannual variability within the Louisiana coastal current: stratification and hypoxia, *J. Mar. Syst.*, *12*(1), 237-248.

Yankovsky, A. E., and D. C. Chapman (1997), A Simple Theory for the Fate of Buoyant Coastal Discharges, *J. Phys. Oceanogr.*, *27*(7), 1386-1401.

Yuan, D., F. Qiao, and J. Su (2005), Cross-shelf penetrating fronts off the southeast coast of China observed by MODIS, *Geophys. Res. Lett.*, *32*(19).

Zavala-Hidalgo, J., S. L. Morey, and J. J. O'Brien (2003), Seasonal circulation on the western shelf of the Gulf of Mexico using a high-resolution numerical model, *J. Geophys. Res*, *108*(C12), 3389.

Zhang, X., S. F. DiMarco, D. C. Smith IV, M. K. Howard, A. E. Jochens, and R. D. Hetland (2009), Near-resonant ocean response to sea breeze on a stratified continental shelf, *J. Phys. Oceanogr.*, *39*(9), 2137-2155.

Zhang, X., R. D. Hetland, M. Marta‐Almeida, and S. F. DiMarco (2012a), A numerical investigation of the Mississippi and Atchafalaya freshwater transport, filling and flushing times on the Texas‐Louisiana Shelf, *J. Geophys. Res*, *117*(C11), C11009.

Zhang, X., M. Marta-Almeida, and R. Hetland (2012b), A high-resolution pre-operational forecast model of circulation on the Texas-Louisiana continental shelf and slope, *J. Oper. Oceanogr.*, *5*(1), 19-34.

Zhang, X., D. C. Smith IV, S. F. DiMarco, and R. D. Hetland (2010), A numerical study of sea-breeze-driven ocean Poincare wave propagation and mixing near the critical latitude, *J. Phys. Oceanogr.*, *40*(1), 48-66.

Zhang, Z., and R. Hetland (2012), A numerical study on convergence of alongshore flows over the Texas-Louisiana shelf, *J. Geophys. Res*, *117*(C11), C11010.